Rewiring of the promoter-enhancer interactome and regulatory landscape in glioblastoma orchestrates gene expression underlying neurogliomal synaptic communication

Chaitali Chakraborty[1,2,*], Itzel Nissen[1,2,*], Craig A. Vincent[1,2], Anna-Carin Hägglund[1,2], Andreas Hörnblad[1] and Silvia Remeseiro[1,2,#]

[1] Umeå Centre for Molecular Medicine (UCMM), Umeå University, Umeå, Sweden.

[2] Wallenberg Centre for Molecular Medicine (WCMM), Umeå University, Umeå, Sweden.

* Equal contribution

\# Corresponding author (lead contact): silvia.remeseiro@umu.se

Abstract

Chromatin organization controls transcription by modulating 3D-interactions between enhancers and promoters in the nucleus. Alterations in epigenetic states and 3D-chromatin organization result in gene expression changes contributing to cancer pathogenesis. Here, we mapped the promoter-enhancer interactome and regulatory landscape of glioblastoma, the most aggressive primary brain tumour. Our data reveals profound rewiring of promoter-enhancer interactions, chromatin accessibility and redistribution of histone marks across the four glioblastoma subtypes. This leads to loss of long-range regulatory interactions and overall activation of promoters, which orchestrate changes in the expression of genes associated to glutamatergic synapses, axon guidance, axonogenesis and chromatin remodeling. SMAD3 and PITX1 emerge as the major transcription factors controlling genes related to synapse organization and axon guidance. Inhibition of SMAD and neuronal activity stimulation cooperate to promote cell proliferation of glioblastoma cells in co-culture with glutamatergic neurons. Our findings provide mechanistic insight into the regulatory networks that mediate neurogliomal synaptic communication.

Introduction

Gene regulation critically relies on regulatory sequences such as enhancers, which control the spatial and temporal specificity of gene expression. In vertebrates, enhancers are often located hundreds of kilobases (kb) to even megabases (Mb) away from their target gene promoters. This long-range action of enhancers over gene promoters is facilitated via the structural organization of the genome in the 3D nuclear space, mainly within sub-megabase domains known as TADs (Topologically Associating Domains)[1,2], which emerge from multiple nested loops by loop extrusion mechanisms[3]. This topological organization of the chromatin allows for physical proximity between enhancers and promoters, constraining the range of action of enhancers and therefore setting the stage for the specificity of promoter-enhancer interactions. Enhancer activity is intimately linked to epigenetic status and, thus, enhancers display different states (i.e., active, silenced, primed or poised) depending on the combination of histone marks and other chromatin features[4–8]. Genome-wide enhancer maps have linked risk variants to disease genes[9], and most genomic variants that predispose to cancer are located in non-coding regions with potential to act as *cis*-regulatory elements[10]. Various evidence supports the role of alterations in the regulatory and topological landscape in different types of cancer. Aberrant super-enhancer function provides oncogenic properties, and cancer cells can acquire super-enhancers to drive expression of oncogenes[11–13]. Proto-oncogenes can become activated by disruption of chromosome insulated neighbourhoods[14], and systematic occurrence of structural rearrangements in *cis*-regulatory elements (e.g., enhancer hijacking) mediates dysregulation in cancer[15,16].

Glioblastoma (GB) (WHO grade IV astrocytoma) is the most malignant form in the wide spectrum of gliomas, the most common primary brain tumours. With a 5-year survival rate of only 3-4%[17], glioblastoma prognosis has not improved considerably in the last decades. Glioblastomas develop rapidly and manifest after a short clinical history of usually less than 3 months[18]. No uniform aetiology has been identified, and mechanistic understanding of GB initiation and progression is difficult given the complexity of genomic, epigenomic, metabolic and microenvironment events contributing to disease. Extensive inter- and intra-tumour heterogeneity are characteristics of glioblastoma that have complicated the finding of specific and targeted therapies.

Epigenetic alterations play a central role in the aetiology of gliomas and are used for molecular classification[19]. In higher-grade gliomas, diverse alterations in genes encoding chromatin remodelers and epigenetics-related enzymes have been described in conjunction with deregulation of the epigenetic landscape and subsequent gene expression alterations[20–22]. Early studies identified four glioblastoma subtypes defined by aberrations and gene expression changes in *EGFR*, *NF1*, and *PDGFRA/IDH1*, corresponding to classical, mesenchymal and neural/proneural subtypes, respectively[23]. Single-cell studies have recently identified that glioblastoma cells display plasticity and transition between four main cellular states influenced by the tumour microenvironment[24]. In the last few years, researchers have begun to integrate transcriptomic analysis with chromatin and epigenetic profiles, DNA methylomes or chromatin architecture data in glioblastomas[25–30], evidencing that glioblastoma is an entity distinguishable from lower grade gliomas. However, despite the efforts to further classify glioblastoma in molecular subtypes and to identify relevant subpopulations, this has not yet been translated into a clinical benefit.

In this study, we apply a multi-omics approach to map the promoter-enhancer interactome and the regulatory landscape of glioblastoma, including histone marks and

chromatin accessibility, in a panel of 15 patient-derived glioblastoma cell lines representing all four expression subtypes and normal human astrocytes as control. We observed a rewiring of the promoter-enhancer interactions, changes in chromatin accessibility and a redistribution of histone marks across all four expression subtypes in glioblastoma. These changes in the regulatory and topological landscapes lead to a significant loss of long-range regulatory interactions and an overall activation of promoter-hubs. This orchestrates changes in the expression of genes associated to synapses, in particular glutamatergic synapses, as well as axon guidance and axonogenesis, and chromatin binding/remodeling. Motif search analysis reveals the transcription factors (TFs) SMAD3 and PITX1 as major direct regulators of a set of downstream target genes related to synaptic contacts and axon guidance. In addition, we functionally demonstrate that inhibition of SMAD3 and stimulation of neural activity additively cooperate to promote proliferation of glioblastoma cells. After the recent discovery of neurogliomal synapses[31–33], that drive tumour progression by relaying neuronal activity to tumour cells, our data offers novel mechanistic insight into the gene regulatory networks that mediate the neurogliomal synaptic communication in glioblastoma.

Results

A map of the regulatory landscape and promoter-enhancer interactome in glioblastoma

To obtain a map of the enhancer landscape and promoter-enhancer interactome in glioblastoma, we performed a multi-omics approach in a panel of 15 patient-derived glioblastoma cell lines alongside normal human astrocytes as a control (Fig. 1a). The 15 patient-derived glioblastoma cell lines were obtained through the human glioblastoma cell culture (HGCC) resource[34], a panel of newly established and well characterized glioblastoma lines derived from GB patient surgical samples, that represent all four expression subtypes (i.e., classical, mesenchymal, neural and proneural). Normal human astrocytes were selected as control since astrocytes are considered to be a cell of origin for glioblastoma[35,36].

We mapped the promoter-enhancer interactome by HiChIP[37], a protein-centric chromatin conformation capture method, using an antibody specific to the promoter mark H3K4me3. Assay for Transposase-Accessible Chromatin with sequencing (ATAC-seq)[38] was used to map chromatin accessibility genome-wide. Via ChIP-seq (Chromatin ImmunoPrecipitation-sequencing) we determined binding sites for histone modifications: the active enhancer mark H3K27ac, the repressive mark H3K27me3, and H3K4me3 predominantly associated to gene promoters. Transcriptome profiling of each line was done by RNA-seq. Our data constitutes a comprehensive map of the regulatory landscape in glioblastoma across all four subtypes, and provides functionally relevant topological information by mapping of the promoter-enhancer interactome (Fig. 1b). In the next sections, we compare the regulatory and topological landscape of glioblastoma to the control astrocytes, while focusing on the features present in all four GB subtypes.

Gene expression changes across all four GB subtypes are associated to synapse organization, glutamatergic synapses and chromatin binding

Transcriptome profiles were obtained for each of the 15 patient-derived cell lines and the normal human astrocytes by bulk RNA-seq. To identify gene expression changes across

all four GB subtypes, we first performed a pair-wise differential expression analysis of each glioblastoma line *vs* the control astrocytes (Fig. 1c and Supplementary Fig. 1a), and then intersected the differentially expressed genes (DEGs) resulting from the 15 pair-wise comparisons (Fig. 1c). We thus identified a set of 497 DEGs that are differentially expressed across all four GB subtypes (Fig. 1d, Supplementary Table S1). Gene Ontology (GO) analysis of this gene set revealed a significant enrichment for terms associated to synapses, and in particular glutamatergic synapses, channel activity and chromatin DNA binding (Fig. 1e). Other GO terms enriched were those related to morphogenesis and development, processes well known to be dysregulated in cancer. A closer analysis of the 497 DEGs showed that 124 genes are annotated as DNA binding, 76 genes encode for Transcription Factors (TFs) and additional 7 genes encode chromatin remodelers (Fig. 1f), evidencing common changes in chromatin-related genes and TFs across the four GB subtypes.

In addition, we detected expression of neurotransmitter receptor genes in all 15 glioblastoma lines (Fig. 1g), including expression of AMPA, kainate, NMDA and mGluR, which are receptors that respond to glutamate, and in accordance with the glutamatergic identity of the neurogliomal synapses[31]. In particular, the kainate receptor gene *GRIK2* and the NMDA receptor gene *GRIN2C* are also differentially expressed across all four GB subtypes in comparison to normal astrocytes. The expression of four known synaptogenesis markers[39] is also detected in our panel of glioblastoma lines (Fig. 1h), in agreement with the emergence of cell subpopulations with synaptogenic properties during glioma progression[40]. Notably, high expression level of the synaptogenesis marker *EFNB2* correlates with lower overall survival of GB patients (TCGA data, Supplementary Fig. 1b), evidencing its clinical relevance in glioblastoma.

Importantly, the 497 DEGs dysregulated across all four subtypes also constitute a gene signature that segregates glioblastoma (GB) from lower grade gliomas (LGG). In a panel of more than 600 tumour samples available at The Cancer Genome Atlas (TCGA), including glioblastoma tumours (GB, n=156) and lower grade gliomas (LGG, n=511), the expression of our 497 DEGs can accurately segregate GB from LGG (Fig. 1i). We then performed a differential expression analysis of the TCGA RNA-seq data from either GB or LGG samples with respect to the corresponding controls, followed by intersection with the 497 DEGs from our data. As a result, we obtained a subset of 127 GB-specific genes and 113 genes "common to all gliomas", the latter resulting from the intersection of both GB gene sets and the LGG gene set (Fig. 1j). Interestingly, GO analysis demonstrated that the 113 genes that are common to all gliomas are preferentially related to morphogenetic and developmental processes, whereas the subset of 127 GB-specific genes is very specifically associated to synapse organization, gliogenesis and glutamate receptor signalling (Fig. 1j). The neurogliomal synapses (i.e., bona fide synapses between presynaptic neurons and postsynaptic glioma cells) utilize glutamate receptors and trigger postsynaptic signals, which in turn affect proliferation and migration of the tumour cells[31–33]. Our analysis reveals that gene expression changes affecting synapses, in particular glutamate receptor signalling, are associated more strongly with glioblastoma samples when compared with lower grade gliomas. This points to certain genes that may be predominant regulators of neural function in glioblastoma pathogenesis.

Loss of long-range regulatory interactions and gain of promoter hub interactions characterise the 3D organisation of the glioblastoma genome

144 Control of transcription is exerted by the physical interaction between enhancers and
145 promoters through a non-linear relationship[41]. To chart these physical interactions
146 genome-wide in glioblastoma, we performed HiChIP with an antibody against the
147 promoter and enhancer mark H3K4me3. We thus obtained a map of the promoter
148 interactome in our panel of glioblastoma lines representing all four subtypes, including
149 not only promoter-enhancer (P-E) but also promoter-promoter (P-P) and enhancer-
150 enhancer (E-E) interactions (Fig. 2a). A comparison of the loops detected by H3K4me3-
151 HiChIP shows that 4316 loops detected in the normal astrocytes are also present in the
152 GB samples, while an additional 5633 are differential loops: 2125 loops are lost (i.e.,
153 astrocyte-specific) and 3508 loops are gained in glioblastoma (i.e., GB-specific) (Fig. 2b).
154 Interestingly, 86.6% of the lost loops involve enhancer interactions (P-E and E-E), while
155 85.4% of the gained loops involve exclusively promoter-promoter (P-P) interactions (Fig.
156 2c). Analysis of only multi-anchor loops (i.e., more than two anchor sites, 78% of total
157 loops) shows that a major fraction of these are gained multi-anchor P-P loops (87.4%,
158 Supplementary Fig. 2a), suggesting that gained P-P interactions in glioblastoma occur
159 mainly in promoter hubs. Importantly, the length of the lost loops (median ~254kb) is
160 significantly higher than that of the gained loops (median ~114kb, p-value=$1.36e^{-290}$),
161 supporting a preferential loss of long-range interactions in glioblastoma (Fig. 2d). These
162 changes in the promoter-enhancer interactome are accompanied by gene expression
163 changes: 183 genes located at the anchors of differential loops are differentially
164 expressed across the 15 patient-derived glioblastoma lines (Supplementary Fig. 2b), out
165 of which 55 (29.7%) encode for transcription factors, chromatin remodelers and other
166 DNA-binding proteins (Fig. 2e). Our map of the enhancer-promoter interactome reveals
167 topological changes that include loss of long-range regulatory interactions and gain of
168 promoter hub interactions in all four glioblastoma subtypes.

169

170 ***Remodeling of the regulatory landscape in glioblastoma is characterized by loss of***
171 ***regulatory elements and activation of promoters***

172 Depending on the combination of histone marks and other chromatin features, enhancers
173 can present different states from active to silenced, primed or poised[4–8]. To map the
174 regulatory landscape in glioblastoma, we profiled by ChIP-seq the binding of H3K27ac
175 (active enhancers), H3K27me3 (polycomb-repressed) and H3K4me3 (promoters and
176 enhancers), together with chromatin accessibility by ATAC-seq (Fig. 2f, Supplementary
177 Table S2). Multiinter intersection of the binding sites in the 15 glioblastoma lines *vs* the
178 control astrocytes, reveals a redistribution of histone marks and changes in chromatin
179 accessibility occurring across the four GB subtypes (Fig. 2g). This is evidenced by the loss
180 of binding sites that were present in astrocytes (i.e., "lost regions") and the remobilization
181 of histone marks to new genomic positions (i.e., "gained regions") in glioblastoma.
182 Similarly, a fraction of the chromatin accessible regions defined by ATAC are altered in
183 glioblastoma. Analysis of genomic annotation of the differential regions shows that the
184 remobilization of histone marks results in a loss of active marks at distant elements and
185 an accumulation at gene promoters, while repressive marks are lost from intergenic
186 regions (Fig. 2h,i).

187 As part of the integration of our multi-omics data genome-wide (Fig. 3a), we used
188 ChromHMM to integrate our datasets and we characterized eight different chromatin
189 states in the normal human astrocytes (Fig. 3b). Plotting the signal of the histone marks
190 and ATAC-seq around the astrocytes' chromatin states displayed clear differences
191 between the glioblastoma lines and the control astrocytes (Fig. 3c-e). H3K27ac signal

increases in poised and weak promoters but decreases around both strong and weak enhancers (Fig. 3d), further supporting the activation of poised/weak promoters and the loss of regulatory activity at enhancers. In addition, the repressive mark H3K27me3 decreases at poised promoters and polycomb-repressed states in glioblastoma (Fig. 3e). These chromatin changes in glioblastoma are also accompanied by increased expression levels at inactive/poised promoters and in the proximity of polycomb-repressed regions (Fig. 3f). Such rewiring of the regulatory landscape, together with the changes in the promoter-enhancer interactome and gene expression levels, supports a loss of long-range regulatory interactions and overall activation of hub promoters across all four GB subtypes.

Remobilization of active chromatin marks around genes associated to glutamatergic synapses, axon guidance and chromatin remodeling

The rewiring in the enhancer landscape in glioblastoma leads to an increased chromatin accessibility and an accumulation of active histone marks at gene promoters. Gene Ontology analysis revealed that those genes near the newly occupied active positions (i.e., gained H3K27ac and ATAC regions) are associated to glutamatergic synapses, axon guidance and axonogenesis, as well as chromatin remodelling/DNA binding (Fig. 4a). Importantly, a major fraction of the genes associated to these biological processes are differentially expressed across the four glioblastoma subtypes (Fig. 4b and Supplementary Fig. 3a). Moreover, the loss of repression (i.e., lost H3K27me3 regions) occurs in the vicinity of genes related to calcium ion homeostasis, ion transport and synaptic transmission (Supplementary Fig. 3b). We therefore observed an accumulation of active marks around genes related to synapses, axon guidance and axonogenesis, and loss of repression of other genes associated to ion transport and synaptic transmission. Altogether, this suggests that the rewiring of the regulatory landscape in glioblastoma orchestrates a series of gene expression changes that contribute to the synaptic communication between neurons and glioma cells.

SMAD3 and PITX1 regulatory networks control synapse organization and axonogenesis in glioblastoma

A search for transcription factor binding site (TFBS) motifs revealed the enrichment of 11 key TFBS motifs within the newly occupied active regions in glioblastoma (Fig. 4c, Supplementary Fig. 3c,d). Not only are the motifs of these 11 TFs enriched in the gained active and open regions, but the genes encoding these 11 TFs are also differentially expressed across all four GB subtypes (i.e., 11 TFs out of the 76 TFs differentially expressed, Fig. 1f). Moreover, a significant fraction of their direct downstream target genes (i.e., motif within a gained peak <2kb TSS) are also differentially expressed in the four GB subtypes (Fig. 4d, Supplementary Fig. 4a). These findings reflect the impact that chromatin mark redistribution and accessibility changes around these TFBS has on gene expression.

GO analysis of the downstream target genes of these 11 TFs points to SMAD3 and PITX1 as major players in the regulatory networks that mediate neurogliomal synaptic communication (Fig. 4e, Supplementary Fig. 4b,c). Various GO terms related to synapse density, postsynaptic organization, axon guidance and axonogenesis are significantly enriched in the case of SMAD3 downstream targets, and in particular glutamatergic synapses for the PITX1 downstream target genes (Fig. 4e). This is in agreement with the

239 reported glutamatergic identity of the neurogliomal synapses[31]. GO terms related to TGFβ
240 receptor activity are significantly enriched among the SIX1 downstream targets (Fig. 4e),
241 which links TGFβ signalling via SMAD3 to the synaptic communication between neurons
242 and glioma cells. Importantly, 70.2% of the SMAD3 target genes differentially expressed
243 in glioblastoma (i.e., 33 out of 47) are also PITX1 downstream targets (Fig. 4d, in bold).
244 The common SMAD3/PITX1 targets include genes encoding semaphorins and ephrins
245 involved in axon guidance[42,43] such as *SEMA5A* and *EPHB3*, the latter of which is also
246 known to participate in the development of excitatory synapses[44]. Other SMAD3/PITX1
247 targets include the transcription factor *NKX2-2* that is involved in regulating axon
248 guidance[45]; *HCN2* and *KCNE4* that encode for gated channels, the latter considered to
249 regulate neurotransmitter release[46]; as well as *TNIK* which is implicated in glutamatergic
250 signalling, where it binds to NMDA receptors and is required for AMPA expression and
251 synaptic function[47].

252 Notably, SMAD3 and PITX1 binding motifs are also located in close proximity (median
253 distance=56bp, Fig. 4f) at the promoters of the 33 common target genes differentially
254 expressed across the four glioblastoma subtypes. In addition, SMAD3 and PITX1 binding
255 motifs are enriched at the anchors of the differential loops in glioblastoma
256 (Supplementary Fig. 3e). Interestingly, Smad proteins have been previously reported to
257 bind CTCF sites in a CTCF-dependent manner in flies[48] and SMAD3 interacts with CTCF in
258 mammalian cells[49]. Apart from SMAD3/PITX1, additional regulatory networks could
259 contribute to a certain extent to the neural role in glioblastoma pathogenesis, since other
260 transcription factors such as EBF1, THRB, EN1, HOXB13 and HOXD10 are also enriched
261 at gained active regions distal to genes involved in axonogenesis and axon guidance (i.e.,
262 motif within a gained peak >2kb TSS) (Supplementary Fig. 4c, Supplementary Fig. 5a).

263 Comparison of *SMAD3-PITX1* and *SMAD3-SIX1* co-expression showed a significant
264 negative correlation between their expression levels, both in our panel of 15 patient-
265 derived samples (Fig. 5a) and in 667 TCGA glioma samples (Fig. 5b). While *SMAD3* is
266 downregulated, *PITX1* and *SIX1* are upregulated in glioblastoma (Fig. 1d). Moreover, low
267 *SMAD3* and high *PITX1* expression levels correlate with lower overall survival in patients
268 (TCGA data, Fig. 5c), pointing to their clinical relevance. It is important to highlight that
269 both the *SMAD3* and *PITX1* loci present topological and regulatory changes (i.e.,
270 differential loops, redistribution of chromatin marks and chromatin accessibility) in
271 comparison to normal astrocytes (Fig. 5d). Also, both *SMAD3* and *PITX1* genes are
272 differentially expressed in all four GB subtypes, and their respective TFBS motifs are
273 enriched at the gained active/open regions at the promoters of genes related to synaptic
274 function, axon guidance and axonogenesis. This altogether indicates the presence of a
275 regulatory network involving SMAD3 and PITX1, and it suggests that they may be the
276 most prominent TFs regulating the neurogliomal synaptic interaction and axonogenesis
277 in glioblastoma.

278

279 ***SMAD3 inhibition and neuronal activity stimulation cooperate to promote cell***
280 ***proliferation in glioblastoma***

281 To functionally support the role of TGFβ signalling and in particular SMAD3 in this
282 context, we tested the effect of their inhibition on the proliferation of glioblastoma cells.
283 First, we induced the reprogramming of glutamatergic neurons (ab259259) from human
284 iPSCs (induced pluripotent stem cells) (Fig. 6a-c), and then established co-cultures of
285 glutamatergic neurons and the glioblastoma line U251-GFP at different time points (Fig.
286 6a,d). By live-cell imaging, we determined the proliferation of the glioblastoma cells in

287 co-culture with glutamatergic neurons upon stimulation of neuronal activity alone or in
288 combination with inhibition of either SMAD3 or the TGFβ receptor ALK5. Treatment with
289 the SMAD3-specific inhibitor SIS3 significantly increases the proliferation of glioblastoma
290 cells in co-culture with glutamatergic neurons, both at early and late time-points (days 6-
291 9 and 14-17, respectively) (Fig. 6e,f). Stimulation of neuronal activity by picrotoxin has
292 only modest effects on U251 proliferation at the highest doses, and only in more mature
293 neurons (day 14-17) (Supplementary Fig. 6a). Importantly, combination of SMAD3
294 inhibition with stimulation of neuronal activity (i.e., SIS3 + picrotoxin) induces
295 proliferation of glioblastoma cells to levels significantly higher than those of SIS3-
296 treatment alone (Fig. 6e,f). This effect in proliferation is not observed upon treatment
297 with the Alk5 inhibitor A83 alone; however, the combination of A83 and picrotoxin also
298 leads to increased proliferation compared to untreated cells (Fig. 6g,h), though to a lesser
299 extent than upon SIS3 treatment. Noteworthy, TGFβ signalling inhibition in combination
300 with picrotoxin treatment only promotes proliferation of the glioblastoma cells in co-
301 culture with glutamatergic neurons, not when cultured in the absence of neurons
302 (Supplementary Figure 6b). In line with our multi-omics data, these functional assays
303 suggest that inhibition of SMAD3 and stimulation of neural activity additively cooperate
304 to promote cell proliferation in glioblastoma cells in co-culture with glutamatergic
305 neurons.

306

307 **Discussion**

308 Up to now, few recent reports had integrated chromatin/epigenetic profiling and
309 transcriptomics in glioblastoma[26–29], and much effort had been put on identifying distinct
310 molecular features of GB subtypes[23,24]. This is of great importance to identify clinically
311 relevant subpopulations with the goal of improving the outcome, however it has not yet
312 resulted into clinical benefits. Here, using a broad panel of patient-derived glioblastoma
313 cell lines and normal human astrocytes as control, we identified changes in the promoter-
314 enhancer interactome, chromatin accessibility and redistribution of histone marks that
315 are present across all four GB expression subtypes (Fig. 6i). Such rewiring of the
316 regulatory landscape and 3D organization of the glioblastoma genome orchestrates gene
317 expression changes which underlie neurogliomal synaptic communication. This is
318 manifested by changes in the expression of genes related to synapse organization, axon
319 guidance and axonogenesis, as well as chromatin binding/remodeling.

320 Chromatin profiling revealed a preferential loss of long-range regulatory loops and
321 reduction of the active mark H3K27ac at strong and weak enhancers in glioblastoma,
322 together with overall activation of promoters, as evidenced by higher enrichment of
323 active marks at poised and weak promoters and reduction of the repressive mark
324 H3K27me3 at those sites. Motif analysis reveals a significant enrichment of SMAD3 and
325 PITX1 sites within gained active and open regions that are located at the promoters of
326 genes related to synapse organization, in particular glutamatergic synapses, axon
327 guidance and axonogenesis. Among the common SMAD3/PITX1 targets, it is worth
328 highlighting genes such as *SEMA5A* and *EPHB3,* classical axon guidance molecules[42,43];
329 the transcription factor *NKX2-2* involved in axon guidance[45]; *HCN2* and *KCNE4* encoding
330 for gated channels; and *TNIK* involved in glutamatergic synaptic function[47]. Moreover,
331 regulatory and topological alterations in the *SMAD3* and *PITX1* loci are accompanied by
332 changes in the expression of both *SMAD3* and *PITX1* genes, which are inversely correlated
333 and associated to lower survival rates in patients. Even if additional transcription factors
334 (i.e., EBF1, THRB, EN1, HOXB13, HOXD10) could contribute by regulating distal genes

335 involved in axonogenesis/axon guidance, our data altogether suggests that SMAD3 and
336 PITX1 act as major direct regulators of a set of downstream target genes related to
337 synapse organization, glutamatergic synapses and axon guidance in glioblastoma.
338 Interestingly, SMAD3 and PITX1 motifs are also significantly enriched at the anchors of
339 differential loops, raising the question of whether they have functions directly linked to
340 chromatin organization. Previous reports have shown that SMAD3 interacts with CTCF in
341 mammalian cells[49], and Smad proteins bind CTCF sites in a CTCF-dependent manner in
342 flies[48]. However, whether PITX1 interacts with CTCF or to what extent SMAD3 and PITX1
343 contribute to 3D chromatin organization are aspects that remain to be explored.

344 The recently discovered neurogliomal synapses provide glutamatergic synaptic input
345 that drives tumour progression[31,32], induces formation of tumour microtubes and speeds
346 up tumour cell invasion by hijacking neuronal migration mechanisms[33]. Importantly,
347 using co-cultures of GB cells and glutamatergic neurons, we functionally demonstrated
348 that inhibition of TGFβ signalling, and specifically SMAD3, in combination with
349 stimulation of neural activity, promotes the proliferation of glioblastoma cells. Cell type-
350 specific transcription factors[50] and epigenomes[51] can modulate SMAD3 downstream
351 targets and therefore orchestrate cell type-specific effects of TGF-β signalling, a pathway
352 which in cancer has dual roles in the regulation of cell death and proliferation depending
353 on the context[52]. This is noteworthy since glioblastoma cells can transition between
354 states under selective pressure (e.g., in response to treatments), which may also result in
355 different effects when comparing different *in vivo* and *in vitro* experimental set-ups. Even
356 though SMAD3 inhibition might reduce cell viability of certain GB subtypes[53], our data
357 underlines the importance of the cellular context, i.e. contacts with neurons, where the
358 combination of neural activity stimulation and SMAD3 inhibition have proven to
359 additively cooperate to promote proliferation of glioblastoma cells (Fig. 6j). Considering
360 these neural-cancer interactions will be pivotal to improve the prognosis of malignancies
361 difficult to treat, such as glioblastoma. Our study thus provides details of the regulatory
362 and topological alterations in glioblastoma and offers novel mechanistic insight into the
363 gene regulatory networks that mediate the neurogliomal synaptic communication.

364

365 Acknowledgements

366 We acknowledge the Biochemical Imaging Center at Umeå University and the National
367 Microscopy Infrastructure, NMI (VR-RFI 2019-00217) for providing assistance in
368 microscopy. Research in SR's laboratory is supported by the Swedish Research Council
369 (2019-01960), the Swedish Cancer Foundation (21 1720), Knut och Alice Wallenbergs
370 Stiftelse (WCMM), the Kempe Foundation (SMK-1964.2) and the Cancer Research
371 Foundation Norrland (AMP 19-977, LP 21-2290, AMP 22-1091). This study is dedicated
372 to the memory of J.M. Remeseiro.

373 Authors contributions

374 CC and IN designed, performed, analysed and interpreted most of the experiments with
375 contributions from CV and AC-H. CV performed and analysed the live-cell imaging
376 experiments. AH co-supervised some bioinformatic analysis, and contributed to data
377 interpretation and manuscript editing. SR designed and supervised the study, secured
378 funding, analysed and interpreted the data, and wrote the manuscript with input from
379 the other authors.

380 These authors contributed equally: CC and IN.

381 Corresponding author: Silvia Remeseiro (silvia.remeseiro@umu.se)

382

383 **References**

384 1. Nora, E. P. *et al.* Spatial partitioning of the regulatory landscape of the X-inactivation
385 centre. *Nature* **485**, 381–385 (2012).

386 2. Dixon, J. R. *et al.* Topological domains in mammalian genomes identified by analysis of
387 chromatin interactions. *Nature* **485**, 376–380 (2012).

388 3. Fudenberg, G. *et al.* Formation of Chromosomal Domains by Loop Extrusion. *Cell*
389 *Reports* **15**, 2038–2049 (2016).

390 4. Ernst, J. *et al.* Mapping and analysis of chromatin state dynamics in nine human cell
391 types. *Nature* **473**, 43–49 (2011).

392 5. Rada-Iglesias, A. *et al.* A unique chromatin signature uncovers early developmental
393 enhancers in humans. *Nature* **470**, 279–283 (2011).

394 6. Calo, E. & Wysocka, J. Modification of enhancer chromatin: what, how, and why? *Mol*
395 *Cell* **49**, 825–37 (2013).

396 7. Cruz-Molina, S. *et al.* PRC2 Facilitates the Regulatory Topology Required for Poised
397 Enhancer Function during Pluripotent Stem Cell Differentiation. *Cell Stem Cell* **20**, 689-
398 705.e9 (2017).

399 8. Crispatzu, G. *et al.* The chromatin, topological and regulatory properties of
400 pluripotency-associated poised enhancers are conserved in vivo. *Nat Commun* **12**, 4344
401 (2021).

402 9. Nasser, J. *et al.* Genome-wide enhancer maps link risk variants to disease genes. *Nature*
403 1–6 (2021) doi:10.1038/s41586-021-03446-x.

404 10. Sur, I. & Taipale, J. The role of enhancers in cancer. *Nat. Rev. Cancer* **16**, 483–493
405 (2016).

406 11. Mansour, M. R. *et al.* Oncogene regulation. An oncogenic super-enhancer formed
407 through somatic mutation of a noncoding intergenic element. *Science* **346**, 1373–1377
408 (2014).

409 12. Hnisz, D. *et al.* Super-enhancers in the control of cell identity and disease. *Cell* **155**,
410 934–947 (2013).

411 13. Bahr, C. *et al.* A Myc enhancer cluster regulates normal and leukaemic haematopoietic
412 stem cell hierarchies. *Nature* **553**, 515–520 (2018).

413 14. Hnisz, D. *et al.* Activation of proto-oncogenes by disruption of chromosome
414 neighborhoods. *Science* **351**, 1454–1458 (2016).

415 15. Weischenfeldt, J. *et al.* Pan-cancer analysis of somatic copy-number alterations
416 implicates IRS4 and IGF2 in enhancer hijacking. *Nat Genet* **49**, 65–74 (2017).

417 16. Xu, J. *et al.* Subtype-specific 3D genome alteration in acute myeloid leukaemia. *Nature*
418 1–12 (2022) doi:10.1038/s41586-022-05365-x.

419 17. Poon, M. T. C., Sudlow, C. L. M., Figueroa, J. D. & Brennan, P. M. Longer-term (≥ 2 years)
420 survival in patients with glioblastoma in population-based studies pre- and post-2005: a
421 systematic review and meta-analysis. *Sci Rep-uk* **10**, 11622 (2020).

422 18. Stewart, B. & WHO, W., C. P. (eds.), International Agency for Research on Cancer,.
423 World Cancer Report 2014. *thehealthwell.info*.

424 19. Louis, D. N. *et al.* The 2021 WHO Classification of Tumors of the Central Nervous
425 System: a summary. *Neuro-oncology* **23**, 1231–1251 (2021).

426 20. Brennan, C. W. *et al.* The somatic genomic landscape of glioblastoma. *Cell* **155**, 462–
427 477 (2013).

428 21. Fontebasso, A. M., Liu, X.-Y., Sturm, D. & Jabado, N. Chromatin Remodeling Defects in
429 Pediatric and Young Adult Glioblastoma: A Tale of a Variant Histone 3 Tail: Chromatin
430 Remodeling Defects in Pediatric and Young Adult Glioblastoma. *Brain Pathol* **23**, 210–216
431 (2013).

432 22. Maleszewska, M. & Kaminska, B. Is Glioblastoma an Epigenetic Malignancy? *Cancers*
433 **5**, 1120–1139 (2013).

434 23. Verhaak, R. G. W. *et al.* Integrated genomic analysis identifies clinically relevant
435 subtypes of glioblastoma characterized by abnormalities in PDGFRA, IDH1, EGFR, and
436 NF1. *Cancer Cell* **17**, 98–110 (2010).

437 24. Neftel, C. *et al.* An Integrative Model of Cellular States, Plasticity, and Genetics for
438 Glioblastoma. *Cell* **178**, 835-849.e21 (2019).

439 25. Mack, S. C. *et al.* Chromatin landscapes reveal developmentally encoded
440 transcriptional states that define human glioblastoma. *J. Exp. Med.* **216**, 1071–1090
441 (2019).

442 26. Chu, T. *et al.* Chromatin run-on and sequencing maps the transcriptional regulatory
443 landscape of glioblastoma multiforme. *Nat Genet* **50**, 1553–1564 (2018).

444 27. Johnston, M. J. *et al.* High-resolution structural genomics reveals new therapeutic
445 vulnerabilities in glioblastoma. *Genome Research* **29**, 1211–1222 (2019).

446 28. Harutyunyan, A. S. *et al.* H3K27M induces defective chromatin spread of PRC2-
447 mediated repressive H3K27me2/me3 and is essential for glioma tumorigenesis. *Nat*
448 *Commun* **10**, 1262 (2019).

449 29. Stępniak, K. *et al.* Mapping chromatin accessibility and active regulatory elements
450 reveals pathological mechanisms in human gliomas. *Nat Commun* **12**, 1–17 (2021).

451 30. Tome-Garcia, J. *et al.* Analysis of chromatin accessibility uncovers TEAD1 as a
452 regulator of migration in human glioblastoma. *Nat Commun* **9**, 4020 (2018).

453 31. Venkataramani, V. *et al.* Glutamatergic synaptic input to glioma cells drives brain
454 tumour progression. *Nature* **573**, 532–538 (2019).

455 32. Venkatesh, H. S. *et al.* Electrical and synaptic integration of glioma into neural circuits.
456 *Nature* **573**, 539–545 (2019).

457 33. Venkataramani, V. *et al.* Glioblastoma hijacks neuronal mechanisms for brain
458 invasion. *Cell* **185**, 2899-2917.e31 (2022).

459 34. Xie, Y. *et al.* The Human Glioblastoma Cell Culture Resource: Validated Cell Models
460 Representing All Molecular Subtypes. *EBioMedicine* **2**, 1351–1363 (2015).

461 35. Azzarelli, R., Simons, B. D. & Philpott, A. The developmental origin of brain tumours: a
462 cellular and molecular framework. *Dev Camb Engl* **145**, dev162693 (2018).

463 36. Yao, M. *et al.* Cellular origin of glioblastoma and its implication in precision therapy.
464 *Cell Mol Immunol* **15**, 737–739 (2018).

465 37. Mumbach, M. R. *et al.* HiChIP: efficient and sensitive analysis of protein-directed
466 genome architecture. *Nat. Methods* **13**, 919–922 (2016).

38. Buenrostro, J. D., Giresi, P. G., Zaba, L. C., Chang, H. Y. & Greenleaf, W. J. Transposition of native chromatin for fast and sensitive epigenomic profiling of open chromatin, DNA-binding proteins and nucleosome position. *Nat. Methods* **10**, 1213–1218 (2013).

39. Dalva, M. B., McClelland, A. C. & Kayser, M. S. Cell adhesion molecules: signalling functions at the synapse. *Nat Rev Neurosci* **8**, 206–220 (2007).

40. Lin, C.-C. J. *et al.* Identification of diverse astrocyte populations and their malignant analogs. *Nat. Neurosci.* **20**, 396–405 (2017).

41. Zuin, J. *et al.* Nonlinear control of transcription through enhancer–promoter interactions. *Nature* **604**, 571–577 (2022).

42. Yu, T. W. & Bargmann, C. I. Dynamic regulation of axon guidance. *Nat Neurosci* **4**, 1169–1176 (2001).

43. Guan, K.-L. & Rao, Y. Signalling mechanisms mediating neuronal responses to guidance cues. *Nat Rev Neurosci* **4**, 941–956 (2003).

44. Dalva, M. B. *et al.* EphB Receptors Interact with NMDA Receptors and Regulate Excitatory Synapse Formation. *Cell* **103**, 945–956 (2000).

45. Holz, A. *et al.* The transcription factors Nkx2.2 and Nkx2.9 play a novel role in floor plate development and commissural axon guidance. *Development* **137**, 4249–4260 (2010).

46. Manville, R. W., Papanikolaou, M. & Abbott, G. W. Direct neurotransmitter activation of voltage-gated potassium channels. *Nat Commun* **9**, 1847 (2018).

47. Coba, M. P. *et al.* TNiK Is Required for Postsynaptic and Nuclear Signaling Pathways and Cognitive Function. *J Neurosci* **32**, 13987–13999 (2012).

48. Bortle, K. V., Peterson, A. J., Takenaka, N., O'Connor, M. B. & Corces, V. G. CTCF-dependent co-localization of canonical Smad signaling factors at architectural protein binding sites in D. melanogaster. *Cell Cycle* **14**, 2677–2687 (2015).

49. Bergström, R. *et al.* Transforming Growth Factor β Promotes Complexes between Smad Proteins and the CCCTC-binding Factor on the H19 Imprinting Control Region Chromatin*. *J Biol Chem* **285**, 19727–19737 (2010).

50. Mullen, A. C. *et al.* Master Transcription Factors Determine Cell-Type-Specific Responses to TGF-β Signaling. *Cell* **147**, 565–576 (2011).

51. Vidakovic, A. T. *et al.* Context-Specific Effects of TGF-β/SMAD3 in Cancer Are Modulated by the Epigenome. *Cell Reports* **13**, 2480–2490 (2015).

52. Ikushima, H. & Miyazono, K. TGFβ signalling: a complex web in cancer progression. *Nat Rev Cancer* **10**, 415–424 (2010).

53. Fan, X. *et al.* Heterogeneity of subsets in glioblastoma mediated by Smad3 palmitoylation. *Oncogenesis* **10**, 72 (2021).

Figure Legends

Figure 1: Gene expression changes common to all four glioblastoma subtypes relate to synapse organization, glutamatergic synapse and chromatin binding. a) Experimental workflow. b) Genomic distribution of HiChIP loops, chromatin accessible regions by ATAC, and H3K27ac, H3K4me3 and H3K27me3 peaks in normal astrocytes and one of the 15 glioblastoma cell lines (U3028). c) Differentially expressed genes (DEGs,

511 red dots) in two representative glioblastoma lines *vs* normal astrocytes (left) and
512 intersection of the 15 pairwise differential expression analysis resulting in 497 DEGs
513 (right). d) Expression of 497 DEGs in all 15 glioblastoma lines and normal astrocytes as
514 determined by RNA-seq (rlog normalized counts). e) Top 10 Gene Ontology terms
515 enriched in the 497 DEGs. f) Number of DEGs annotated as DNA-binding, transcription
516 factors or chromatin remodelers. g-h) Expression of neurotransmitter receptor genes (g)
517 and synaptogenesis markers (h) in the 15 glioblastoma lines. i) Sample-to-sample
518 distance for TCGA samples annotated as GB (glioblastoma, n=156) or LGG (lower grade
519 glioma, n=511). j) Intersections between our 497 DEGs and the differentially expressed
520 genes from TCGA tumour samples, either GB *vs* normal or LGG *vs* normal tissue (left). Top
521 10 GO terms enriched in the 127 GB-specific genes or 113 genes common to GB and LGG
522 (right).

523 **Figure 2: Loss of long-range regulatory interactions and changes in the regulatory**
524 **landscape in glioblastoma.** a) Distribution of HiChIP loops and H3K4me3 peaks in a
525 region of chromosome 2. b) Intersection of HiChIP loops in the 15 glioblastoma lines and
526 normal astrocytes defines lost loops ("astrocyte-specific") and gained loops ("GB-
527 specific") in glioblastoma. c) Annotation of lost and gained loops as P-P, P-E or E-E loops.
528 d) Length (bp) of lost and gained loops (t-test, Benjamini correction). e) Number of DEGs
529 at the anchors of differential loops annotated as DNA-binding, transcription factors or
530 chromatin remodelers. f) Read distribution of histone marks and ATAC around the
531 indicated ±10kb regions in astrocytes and three representative glioblastoma lines. g)
532 Redistribution of histone marks and ATAC regions in glioblastoma. h) Genomic
533 annotation of differential histone peaks and ATAC regions in glioblastoma *vs* normal
534 astrocytes. i) H3K27ac peak count frequency around the TSSs.

535 **Figure 3: Remodeling of the regulatory landscape in glioblastoma includes**
536 **reduction of active marks at enhancers and activation of promoters.** a) Genome-
537 wide integration of all the multi-omics data. b) Chromatin states defined by chromHMM
538 in normal astrocytes. c) Read distribution of histone marks and ATAC across the various
539 chromatin states in astrocytes and three representative glioblastoma lines. d-f) Density
540 plots representing the normalized H3K27ac (d), H3K27me3 (e) and RNA-seq (f) signal
541 around the astrocytes' chromatin states in glioblastoma (blue) *vs* astrocytes (red).

542 **Figure 4: SMAD3 and PITX1 regulatory networks control genes associated to**
543 **(glutamatergic) synapse organization and axonogenesis in glioblastoma.** a) Top 25
544 GO terms enriched for genes proximal to gained active and open regions in glioblastoma
545 (peaks <2kb TSS). b) Expression of DEGs related to synapse and glutamatergic synapse
546 (top), and axon guidance and axonogenesis (bottom) located <2kb from a gained
547 active/open peak. c) Intersection of the 497 DEGs with the HOMER significantly enriched
548 motifs at the gained regions or anchors of differential loops identifies 11 key TFs. d)
549 Expression of PITX1 and SMAD3 downstream target genes (i.e., motif enrichment at a
550 differential peak <2kb TSS) among the DEGs in glioblastoma *vs* normal astrocytes
551 (common targets in bold). e) Top GO terms enriched for SMAD3, PITX1 and SIX1 proximal
552 downstream target genes. f) Distance between SMAD3 and PITX1 motifs at the promoters
553 of the 33 common SMAD3/PITX1 target genes (left, median=56bp) *vs* background model
554 (right, median=124bp). (Wilcoxon test).

555 **Figure 5: Regulatory alterations in the *SMAD3* and *PITX1* loci accompanied by**
556 **inversely correlated gene expression and association to lower survival in patients.**
557 a-b) Scatterplots showing co-expression of SMAD3-PITX1 (left) or SMAD3-SIX1 (right)
558 expressed as normalized counts in our data (a) and TCGA datasets (b) (Pearson

559 correlations). c) Kaplan-Meier survival curves plotted for patients stratified by quartiles
560 of SMAD3 or PITX1 expression (TCGA data) (log-rank Mantel-Cox test). d) Changes in the
561 enhancer landscape and promoter-enhancer interactome at the SMAD3 and PITX1 loci
562 (U3028 depicted as representative glioblastoma line).

563 **Figure 6: SMAD3 inhibition and neuronal activity cooperate to promote**
564 **proliferation of glioblastoma cells in co-culture with glutamatergic neurons.** a)
565 Workflow to reprogram glutamatergic neurons from iPSCs, establish a co-culture with
566 GFP-labelled U251 glioblastoma cells and live-cell image acquisition. b) Photomicrograph
567 of glutamatergic neurons at days 3, 7 and 12. c) Glutamatergic neurons stained with an
568 antibody against β3-Tubulin (red) (DAPI, blue). d) Photomicrographs of glutamatergic
569 neurons and U251-GFP glioblastoma cells (green) in co-culture. e,g) Proliferation curves
570 depicting the growth of U251 cells (measured as normalized GFP integrated intensity) in
571 co-culture with glutamatergic neurons in the 72h after seeding at day 6 (left) or day 14
572 (right), while treated with either the SMAD3-specific inhibitor SIS3 (e) or the ALK5
573 inhibitor A83 (g), in combination with increasing concentrations of picrotoxin. (Multiple
574 unpaired t-test, t=72h, (* $p<0.01$, ** $p<0.005$, *** $p<0.000005$, n=6-8=). f,h)
575 Representative images from the live-cell imaging proliferation assay of U251-GFP in co-
576 culture with glutamatergic neurons, in the presence of either SIS3 (f) or A83 (h). i)
577 Scheme illustrating the regulatory and topological changes in the glioblastoma genome
578 including loss of long-range interactions, gain of promoter-promoter loops,
579 redistribution of active chromatin marks towards SMAD3 and PITX1 binding motifs and
580 upregulation of genes related to synapse organization, axon guidance and axonogenesis.
581 j) Illustration depicting that Smad3 inhibition and stimulation of neural activity
582 cooperate to promote proliferation of glioblastoma cells in co-culture with glutamatergic
583 neurons.

584 **Supplementary Figure 1:** a) MA plots showing genes differentially expressed (DEGs, red
585 dots) in each of the 15 glioblastoma lines *vs* normal astrocytes. b) Kaplan-Meier survival
586 curves plotted for patients stratified by quartiles of *EFNB2* expression (TCGA data) (log-
587 rank Mantel-Cox test).

588 **Supplementary Figure 2:** a) Annotation of lost and gained multi-anchor loops as
589 promoter-promoter, promoter-enhancer or enhancer-enhancer loops. b) Expression of
590 45 DEGs located at the anchors of lost loops (left) and 138 DEGs at the anchors of gained
591 loops (right), in all 15 glioblastoma lines and normal astrocytes as determined by RNA-
592 seq (rlog normalized counts).

593 **Supplementary Figure 3:** a) Expression of DEGs related to chromatin remodelling and
594 DNA binding located <2kb from a gained active/open peak. b) Top 25 GO terms enriched
595 for the genes proximal to the lost repressive regions in glioblastoma (peaks <2kb TSS).
596 c,d) Summary of the TF binding motifs enriched at proximal (<2kb TSS) (c) or distal (>2kb
597 TSS) (d) gained regions in glioblastoma for H3K27ac, ATAC and H3K4me3, including
598 motif, sequence and p-values. e) Summary of the TF binding motifs enriched at the
599 anchors of the differential loops, including motif, sequence and p-value.

600 **Supplementary Figure 4:** a) Expression of the SIX1, EN1, GSC, HOXD10, HOXB13 and
601 LHX2 downstream target genes (i.e., motif enrichment at a differential peak <2kb TSS)
602 that are DEGs in glioblastoma *vs* normal astrocytes. b) GO terms enriched for the GSC,
603 EBF1, HOXD10, EN1 and HOXB13 proximal downstream target genes (<2kb TSS). c) GO
604 terms enriched for the PITX1 and SMAD3 distal downstream target genes (>2kb TSS).

605 **Supplementary Figure 5:** a) GO terms enriched for the EBF1, EN1, THRB, GSC, LHX2,
606 HOXB13, HOXD10 and SIX1 distal downstream target genes (>2kb TSS).

607 **Supplementary Figure 6:** a) Proliferation curves depicting the growth of U251 cells
608 (measured as normalized GFP integrated intensity) in co-culture with glutamatergic
609 neurons in the 72h after seeding at day 6 (left) or day 14 (right) at different
610 concentrations of picrotoxin. (Multiple unpaired t-test, t=72h, (* $p<0.01$, ** $p<0.005$, ***
611 $p<0.000005$). (n=6-8). b) Proliferation curves of U251 cells in the absence of neurons
612 (measured as normalized cell count) in the 72h after seeding at day 6 (left) or day 14
613 (right) and under the same drug treatments as used in Figure 6e,g.

614

615

616 # Methods

617

618 ## *Cell Culture*

619 *Human glioblastoma cell lines* were derived from glioblastoma (GB) patient biopsies and
620 obtained via the Human Glioblastoma Cell Culture (HGCC) resource[1] (Uppsala University,
621 Sweden). The 15 patient-derived glioblastoma lines represent the four GB expression
622 subtypes (n=5 classical, n=5 mesenchymal, n=3 pro-neural and n=2 neural). Cells were
623 seeded onto poly-ornithine/laminin-coated plates and grown in Feed Medium (1:1 ratio
624 of DMEM/F12 Glutamax (Gibco) and Neurobasal medium (Gibco), supplemented with 1X
625 B27 (Gibco), 1X N-2 Supplement (Gibco), 1% penicillin/ streptomycin (Gibco), 10 ng/ml
626 EGF (Epithelial Growth Factor; PreproTech EC Ltd.) and 10 ng/ml FGF (Fibroblast
627 Growth Factor; PeproTech EC Ltd).

628 *Normal Human Astrocytes* (Lonza, CC-2565) were grown in AGM Astrocyte Growth
629 medium BulletKit (Lonza, CC-3186).

630 *U251 glioblastoma cells* (Sigma-Aldrich, #09063001) were grown in EMEM (EBSS)
631 supplemented with 2mM Glutamine, 1% NEAA (Non-Essential Amino Acids), 1mM
632 Sodium Pyruvate, 10% FBS (Fetal Bovine Serum) and 1% penicillin/streptomycin (all
633 from Gibco). The GFP-labelled U251 line was established by lentiviral integration of the
634 GFP reporter gene.

635 The *iPSC-derived glutamatergic neurons* (ioGlutamatergic neurons) were purchased from
636 Abcam (ab259259), where human iPSCs were exposed to a 3-day induction protocol (day
637 -3 to 0) and ioGlutamatergic neurons were cryopreserved. Upon thawing, 11 000
638 ioGlutamatergic neurons per well were seeded onto a PDL-Geltrex-coated 96-well plates
639 and grown in Complete Glutamatergic Neuron Medium (CGNM) i.e., Neurobasal medium
640 (Gibco) supplemented with 1X Glutamax (Gibco), 25μM 2-mercaptoethanol (Gibco), 1X
641 B27 (Gibco), 10 ng/ml NT3 (R&D) and 5 ng/ml BDNF (R&D). During the stabilization
642 phase, the CGNM was supplemented with 1 μg/ml doxycycline (Sigma) during 96h (day
643 0-4) and DAPT (Sigma) for 48h (day 2-4) for sustained induction. During the maintenance
644 phase (day 4 onwards), the ioGlutamatergic neurons were grown in CGNM (without
645 doxycycline and DAPT) with a half-medium change regime every 48 hours.

646 To establish the *co-culture of glutamatergic neurons and glioblastoma cells*, 5 000 U251-
647 GFP glioblastoma cells were seeded onto the glutamatergic neurons either at day 6 or day
648 14 of culture. The co-cultures were treated with Picrotoxin (10, 25 or 33 μM, TOCRIS
649 #1128), SIS3 (10 μM, Calbiochem #566405), A83 (0.5 μM, Sigma SML0788) or
650 combinations of Picrotoxin and SIS3/A83. Live-cell imaging was performed on an

651 IncuCyte S3 Live-Cell Analysis instrument (Sartorius) and proliferation of the GFP-
652 labelled U251 cells was determined by measuring GFP integrated intensity using the
653 Incucyte Base Analysis Software. Data points in Figure 6e,g and Supplementary Figure 6
654 correspond to n=6-8 replicates per condition and timepoint, for which 4 fields were
655 imaged, and values are normalized to t=0. Significant differences in cell proliferation were
656 assessed using unpaired t-test with correction for multiple testing at t=72h (* $p<0.01$, **
657 $p<0.005$, *** $p<0.000005$).

658 All cell lines were grown in a cell incubator at 37°C in a humidified atmosphere (95%
659 humidity) with 5% CO2.

660

661 ***RNA-seq***

662 RNA-seq was performed in 15 glioblastoma cell lines and normal human astrocytes. Total
663 RNA was extracted using RNeasy Plus Mini Kit (Qiagen, #74134) in technical duplicates
664 for each cell line. Poly(A) RNA was purified using the NEBNext Poly(A) mRNA Magnetic
665 Isolation Module (CAT #E7490L). RNA-seq libraries were prepared using the NEBNext®
666 Ultra™ II RNA Library Prep Kit for Illumina (CAT# E7770L) and NEBNext® Multiplex
667 Oligos for Illumina® (96 Unique Dual Index Primer Pairs) (CAT #E6440S) following the
668 manufacturer's instructions (8 amplification cycles). The RNA-seq libraries were
669 sequenced on a NovaSeq 6000 Sequencing System (Illumina) obtaining in average
670 ~53 million 150PE reads per library.

671

672 <u>*RNA-seq analysis*</u>

673 Fastq files were quality-checked with FastQC (https:// www.bioinformatics.babraham.
674 ac.uk/projects/fastqc/) and raw reads were mapped to the human genome
675 (GRCh38/hg38) using STAR (2.7.6a)[2]. Genes with a minimum row sum of 10 reads were
676 kept for further analysis. Normalization and differential expression analysis of each
677 glioblastoma line *vs* the control normal astrocytes were performed using DESeq2 ($p<0.01$
678 and FDR<0.01), and the DEGs resulting from the 15 pair-wise comparisons were then
679 intersected using the UpSet command from the ComplexHeatmap package, resulting in
680 497 differentially expressed genes (DEGs) across all 15 glioblastoma lines. Pheatmap
681 package was used for clustering of differentially expressed genes in figures 1d, 4b, 4d,
682 and supplementary figures 2b, 3a and 4a. Gene Ontology (GO) and KEGG enrichment
683 analysis were performed using clusterProfiler ($p<0.01$ and FDR<0.01)[3] (CC: cellular
684 component, MF: molecular function, BP: biological process). RNA-seq data available at
685 The Cancer Genome Atlas (TCGA) from both human Glioblastoma (GB, n=156) and Low-
686 Grade Glioma (LGG, n=511) tissue samples were retrieved using the R packages
687 TCGAbiolinks and RTCGAToolbox, together with normal tissue samples. We calculated
688 Euclidean distances among the tumour samples based on the gene expression of our 497
689 DEGs and plotted the sample-to-sample distances as a heatmap. The differential
690 expression analysis of either GB samples or LGG samples *versus* the respective normal
691 control tissues was performed using DESeq2 (FDR<0.01). The UpSet command from the
692 ComplexHeatmap package was used to intersect the 497 DEGs from our data with the
693 DEGs resulting from the TCGA-GB *vs* Normal and TCGA-LGG *vs* Normal differential
694 expression analysis, and the intersection was represented as an UpSet plot. Co-
695 expression analysis for *SMAD3-PITX1* and *SMAD3-SIX1* gene pairs and Pearson
696 correlation was calculated and plotted on R and ggplot2, using the rlog normalized counts
697 for our RNA-seq data and the vsd log2 normalized counts for the TCGA data.

698

699 ***ChIP-seq***

700 ChIP-seq was performed in 15 glioblastoma cell lines and normal human astrocytes as
701 described before[4,5] with some modifications. Briefly, cells were fixed on the plate by
702 adding formaldehyde directly to the medium (final concentration 1% formaldehyde) for
703 15 minutes at room temperature while rotating. The crosslinking reaction was quenched
704 by adding Glycine (final concentration 125mM Glycine) for 5 min, and fixed cells were
705 scraped off and harvested in 1X cold PBS containing protease inhibitors. Cells were then
706 resuspended in lysis buffer (3-6x10^6 cells/ml) and sonicated in a Covaris E220
707 instrument (shearing time 12min, PIP 140, duty factor 5, 200 cycles per burst), to achieve
708 a fragment size ranging from 200bp to 700bp. Chromatin immunoprecipitation was
709 performed with antibodies against H3K27ac (ab4729), H3K4me3 (ab8580) and
710 H3K27me3 (ab192985), and using Dynabeads™ M-280 Sheep Anti-Rabbit IgG
711 (Invitrogen 11203D). H3K27ac and H3K27me3 ChIP–seq libraries were prepared using
712 the NEBNext Ultra II DNA Library Prep Kit for Illumina (E7645L) and NEBNext®
713 Multiplex Oligos for Illumina® (E6440S). The H3K4me3 library was prepared using Accel
714 NGS 2S Plus DNA Library Prep (#21024, Swift Biosciences) and indexing Kit (#26596,
715 Swift Biosciences), since it was processed and sequenced together with the H3K4me3-
716 HiChIP. ~10ng of immunoprecipitated chromatin (as quantitated by the Qubit
717 fluorometer) alongside the corresponding inputs were amplified for 8 cycles and further
718 processed according to the guidelines of the library prep kits. SPRI Select beads (Beckman
719 Coulter) were used for clean-up and size selection. The ChIP-seq libraries were
720 sequenced on a NovaSeq 6000 Sequencing System (Illumina) obtaining in average
721 ~51 million 150PE reads per library.

722

723 <u>*ChIP-seq analysis*</u>

724 Fastq files were quality-checked with FastQC (https:// www.bioinformatics.babraham.
725 ac.uk/projects/fastqc/) and raw reads were mapped to the human genome
726 (GRCh38/hg38) using bowtie2 (2.4.1)[6] (--threads 4 --very-sensitive). Peak calling was
727 performed by MACS2[7] (options: --broad -g hs -B -q 0.05 -f BAMPE) using the
728 corresponding input track as control (i.e. astrocytes *vs* astrocyte input, and each of the
729 glioblastoma cells *vs* the corresponding input depending on the subtype i.e., CL-input, MS-
730 input, PN-input or NL-input). ChIP-seq signal was plotted as heatmaps using plotHeatmap
731 from deepTools. Bigwig files were visualized in the UCSC genome browser
732 (https://genome.ucsc.edu/). Density plots displaying the signal around TSSs or defined
733 chromatin states were performed with plotProfile upon calculation of enrichment using
734 computeMatrix. Bedtools multiinter tool was used to determine the regions that were lost
735 or gained in glioblastoma for each of the histone marks. Lost regions were defined as
736 astrocyte-specific regions (i.e. present in astrocytes and absent in all 15 glioblastoma
737 lines), while gained regions were defined as glioblastoma-specific (i.e. absent in
738 astrocytes and present in at least 10 out of 15 glioblastoma lines). Genomic annotations
739 of peaks as well as lost and gained regions were obtained using
740 BSgenome.Hsapiens.UCSC.hg38, ChIPpeakAnno, ChIPseeker[8] & EnsDb.Hsapiens.v86 in R.
741 Gene Ontology analysis of genes proximal (<2kb TSS) or distal (>2kb TSS) to the
742 gained/lost regions were performed using clusterProfiler[3] (CC: cellular component, MF:
743 molecular function, BP: biological process). Search for TFBS (transcription factor binding
744 sites) motifs was conducted using HOMER (v4.11) tool findMotifsGenome.pl. For each
745 histone mark, motif analysis was performed within the differential regions located either

746 proximally (<2kb) or distally (>2kb) to TSSs. Significantly enriched TF motifs (p<0.01)
747 were intersected with the 497 DEGs to identify transcription factors that were
748 differentially expressed and whose motifs were enriched at the differential histone
749 regions. Distances between SMAD3 and PITX1 motifs at the promoters of the 33 common
750 SMAD3/PITX1 target genes were calculated within the differential regions (i.e., gained
751 H3K27ac and ATAC peaks) located <2kb of TSS, and using as background model the
752 common peaks at promoters genome-wide. Discovery of chromatin states in normal
753 astrocytes was performed with ChromHMM[9] using the H3K27ac, H3K4me3, H3K27me3,
754 ATAC-seq and RNA-seq datasets as input and setting 8 state emissions.

755

756 ***ATAC-seq***

757 ATAC-seq was performed in 15 glioblastoma cell lines and normal human astrocytes
758 (50 000 cells/sample) as previously described[10,11]. Briefly, DNA tagmentation was
759 performed 30 minutes at 37°C using the Illumina Tagment DNA TDE1 Enzyme and Buffer
760 Kits (#20034197). The reaction was purified using a MinElute Purification Kit (Qiagen
761 #28004) and fragmentation was assessed via Bioanalyzer High Sensitivity DNA Analysis
762 (Agilent # 5067-4626). 5µl of tagmented DNA per library were amplified for 13 cycles
763 using NEBNext High-Fidelity 2x PCR Master Mix (M0541S) and custom oligonucleotides
764 (for oligo sequences see Supplementary Table S3). The ATAC libraries were sequenced
765 on a NovaSeq 6000 Sequencing System (Illumina) aiming ~55 million 150PE reads per
766 library.

767

768 *ATAC-seq Analysis*

769 ATAC-seq analysis was performed according to the ENCODE ATAC-seq Processing
770 Pipeline with some modifications. Fastq files were quality-checked with FastQC (https://
771 www.bioinformatics.babraham. ac.uk/projects/fastqc/). The pipeline for further
772 processing included trimming with cutadapt to remove the Nextera adaptor sequence
773 CTGTCTCTTATACACATCT, mapping to the human genome (GRCh38/hg38) using
774 bowtie2[6] (--k 2, --threads 8, --local, --maxins 2000), removing duplicates with
775 MarkDuplicates from Picard toolbox and filtering with samtools to keep high quality and
776 uniquely aligned read pairs. Peak calling was performed using MACS2[7] (--broad -q 0.05 -
777 -shift 100 --extSize 200 against baseline). Genomic annotations of peaks were obtained
778 using ChIPseeker[8]; the ATAC-seq signal was plotted as heatmaps using plotHeatmap from
779 deepTools, and bigwig files were visualized in the UCSC genome browser
780 (https://genome.ucsc.edu/). Density plots displaying the signal around defined
781 chromatin states were performed with plotProfile upon calculation of enrichment using
782 computeMatrix. Bedtools multiinter tool was used to determine the ATAC regions that
783 were lost or gained in glioblastoma. Lost regions were defined as astrocyte-specific
784 regions (i.e. present in astrocytes and absent in all 15 glioblastoma lines), while gained
785 regions were defined as glioblastoma-specific (i.e. absent in astrocytes and present in at
786 least 10 out of 15 glioblastoma lines). Lost and gained ATAC regions were then annotated
787 using BSgenome.Hsapiens.UCSC.hg38, ChIPpeakAnno, ChIPseeker[8] &
788 EnsDb.Hsapiens.v86 in R. Gene Ontology analysis of genes proximal (<2kb TSS) or distal
789 (>2kb TSS) to the gained/lost ATAC regions were performed using clusterProfiler (CC:
790 cellular component, MF: molecular function, BP: biological process). Search for TFBS
791 (transcription factor binding sites) motifs was conducted using HOMER (v4.11) tool
792 findMotifsGenome.pl. Motif analysis was performed within the differential ATAC regions

located either proximally (<2kb) or distally (>2kb) to TSSs. Significantly enriched TF motifs ($p<0.01$) were intersected with the 497 DEGs to identify transcription factors that were differentially expressed and whose motifs were enriched at the differential ATAC regions.

HiChIP

HiChIP was performed in 15 glioblastoma cell lines and normal human astrocytes using the Arima-HiC+ Kit (A101020) and following the guidelines in the Arima-HiChIP user guide for mammalian cells. 9-15x10^6 cells per line were used to obtain at least 12-15µg of input DNA for HiChIP. Cells were fixed in 1% formaldehyde for 15 min at room temperature while rotating, and crosslinking reaction was quenched by adding Glycine (final concentration 125mM Glycine) for 5 min. Subsequent steps included digestion of crosslinked chromatin with restriction enzymes, end-filling with biotinylated nucleotides and ligation. Proximally ligated chromatin was then sheared on a Covaris E22O instrument (shearing time 5min, PIP 105, duty factor 5, 200 cycles), to achieve a fragment size ranging from 200bp to 800bp. Chromatin immunoprecipitation was performed with an antibody against H3K4me3 (ab8580). After biotin enrichment and adapters ligation, immunoprecipitated DNA was subjected to PCR amplification (8-11 cycles) using Accel-NGS 2S Plus DNA Library Kit (#21024, Swift Biosciences) and indexing Kit (#26696, Swift Biosciences), according to the Arima-HiChIP Library Prep user guide. Quality controls for chromatin digestion, ligation, shearing and library preparation were assessed via Bioanalyzer High Sensitivity DNA Analysis (Agilent # 5067-4626) and passed prior to sequencing. The HiChIP libraries were sequenced on a NovaSeq 6000 Sequencing System (Illumina) aiming ~100 million 150PE reads per library.

HiChIP analysis

HiChIP analysis was performed as described before[12] using HiC-Pro and Hichipper. Fastq files were quality-checked with FastQC (https:// www.bioinformatics.babraham.ac.uk/projects/fastqc/). Mapping to the human genome (GRCh38/hg38) and retrieval of valid interacting fragments was performed using the HiC-Pro software v3.1.0 and setting ligation sites as GATCGATC, GANTGATC, GANTANTC, GATCANTC. Valid loops were identified using Hichipper v.0.7.3. Significant loops were determined using diffloop (1.20.0)[13] in R filtering for a minimum normalized read pair (loop count ≥ 2), FDR<0.01 and loop length ≥ 5000 bp. HiChIP samples passed quality control if ≥ 4000 significant loops were detected. To identify the differential loops, we defined lost and gained loops in glioblastoma as astrocyte-specific and GB-specific loops, respectively. The criteria were set such as lost loops are those present in normal astrocytes and absent in all glioblastoma lines{i.e., ∃ astrocytes (counts ≥2) & ∄ 14/14 GB (counts=0)}, while gained loops are absent in normal astrocytes and present in at least 8 out of the 14 glioblastoma lines{i.e., ∄ astrocytes (counts=0) & ∃ 8/14 GB (counts≥2)}. Annotation of the significant and differential loops were done using GenomicInteractions package in R (1.26.0). Loops were categorized as promoter-promoter (P-P), promoter-enhancer (P-E) or enhancer-enhancer (E-E) setting the criteria for promoter regions <2kb TSS and considering E-E as distal-distal regions. Differences in loop length (bp) between lost and gained loops were assessed using a t-test with Benjamini-Hochberg correction. Among the differential loops, multi-anchor loops were identified as loops that share anchors with other loop(s) i.e., one anchor is utilized by two or more loops. Search for TFBS (transcription factor binding

sites) motifs was conducted using HOMER (v4.11) tool findMotifsGenome.pl. Motif analysis was performed within the anchors of the differential lost and gained loops. Significantly enriched TF motifs ($p<0.01$) were intersected with the 497 DEGs to identify transcription factors that were differentially expressed and whose motifs were enriched at the anchors of the differential loops.

Statistical analysis

Statistical tests used are indicated in the corresponding Methods sections and in figure legends. Differences in loop length (bp) between lost and gained loops were assessed using a t-test with Benjamini-Hochberg correction. Kaplan-Meier survival curves were plotted for patients stratified by quartiles of expression and tested using a log-rank Mantel-Cox test. Differences in SMAD3/PITX1 motif distance were assessed using a Wilcoxon test. Differences in cell proliferation were determined using unpaired t-test with correction for multiple testing (* $p<0.01$, ** $p>0.005$, *** $p<0.000005$).

Bioinformatic analyses and graphics

Most statistical analysis related to RNA-seq, ChIP-seq, ATAC-seq and HiCHIP were performed within the R environment (v.4.0.0-v.4.1.2) using basic built-in functions and publicly available packages dplyr, plyr, reshape2, ggmisc, ggpubr (R-CRAN). DESeq2, ComplexHeatmap, ClusterProfiler, BSgenome.Hsapiens.UCSC.hg38, ChIPpeakAnno, ChIPseeker and EnsDb.Hsapiens.v86 are open source tools available via Bioconductor (https://www.bioconductor.org/). Data in figures 1d, 2c, 2e, 2h, 5c, 6e, 6g and supplementary figures 2a and 6a,b were plotted using GraphPad Prism 9. The Circos Plot in figure 3a was generated using RCircos (R-CRAN package: 1.2.0). All other plots were created using basic R graphical interface and ggplot2. Genomic snapshots were downloaded from UCSC Genome Browser visualizations (https://genome.ucsc.edu/).

Data availability

The RNA-seq, ChIP-seq, ATAC-seq and HiChIP datasets generated in this study have been deposited in GEO (Gene Expression Omnibus) under the accession number GSE217349.

Methods References

1. Xie, Y. *et al.* The Human Glioblastoma Cell Culture Resource: Validated Cell Models Representing All Molecular Subtypes. *EBioMedicine* **2**, 1351–1363 (2015).

2. Dobin, A. *et al.* STAR: ultrafast universal RNA-seq aligner. *Bioinformatics* **29**, 15–21 (2013).

3. Wu, T. *et al.* clusterProfiler 4.0: A universal enrichment tool for interpreting omics data. *Innovation* **2**, 100141 (2021).

4. Remeseiro, S., Cuadrado, A., Gomez-Lopez, G., Pisano, D. G. & Losada, A. A unique role of cohesin-SA1 in gene regulation and development. *EMBO J.* **31**, 2090–2102 (2012).

5. Cuadrado, A., Remeseiro, S., Graña, O., Pisano, D. G. & Losada, A. The contribution of cohesin-SA1 to gene expression and chromatin architecture in two murine tissues. *Nucleic Acids Res.* **43**, 3056–3067 (2015).

883 6. Langmead, B. & Salzberg, S. L. Fast gapped-read alignment with Bowtie 2. *Nat Methods*
884 **9**, 357–359 (2012).

885 7. Zhang, Y. *et al.* Model-based analysis of ChIP-Seq (MACS). *Genome Biol* **9**, R137 (2008).

886 8. Yu, G., Wang, L.-G. & He, Q.-Y. ChIPseeker: an R/Bioconductor package for ChIP peak
887 annotation, comparison and visualization. *Bioinformatics* **31**, 2382–2383 (2015).

888 9. Ernst, J. & Kellis, M. Chromatin-state discovery and genome annotation with
889 ChromHMM. *Nat Protoc* **12**, 2478–2492 (2017).

890 10. Buenrostro, J. D., Giresi, P. G., Zaba, L. C., Chang, H. Y. & Greenleaf, W. J. Transposition
891 of native chromatin for fast and sensitive epigenomic profiling of open chromatin, DNA-
892 binding proteins and nucleosome position. *Nat. Methods* **10**, 1213–1218 (2013).

893 11. Buenrostro, J. D., Wu, B., Chang, H. Y. & Greenleaf, W. J. ATAC-seq: A Method for
894 Assaying Chromatin Accessibility Genome-Wide. *Curr Protoc Mol Biol* **109**, 21.29.1-
895 21.29.9 (2015).

896 12. Mumbach, M. R. *et al.* HiChIP: efficient and sensitive analysis of protein-directed
897 genome architecture. *Nat. Methods* **13**, 919–922 (2016).

898 13. Lareau, C. A. & Aryee, M. J. diffloop: a computational framework for identifying and
899 analyzing differential DNA loops from sequencing data. *Bioinformatics* **34**, 672–674
900 (2018).

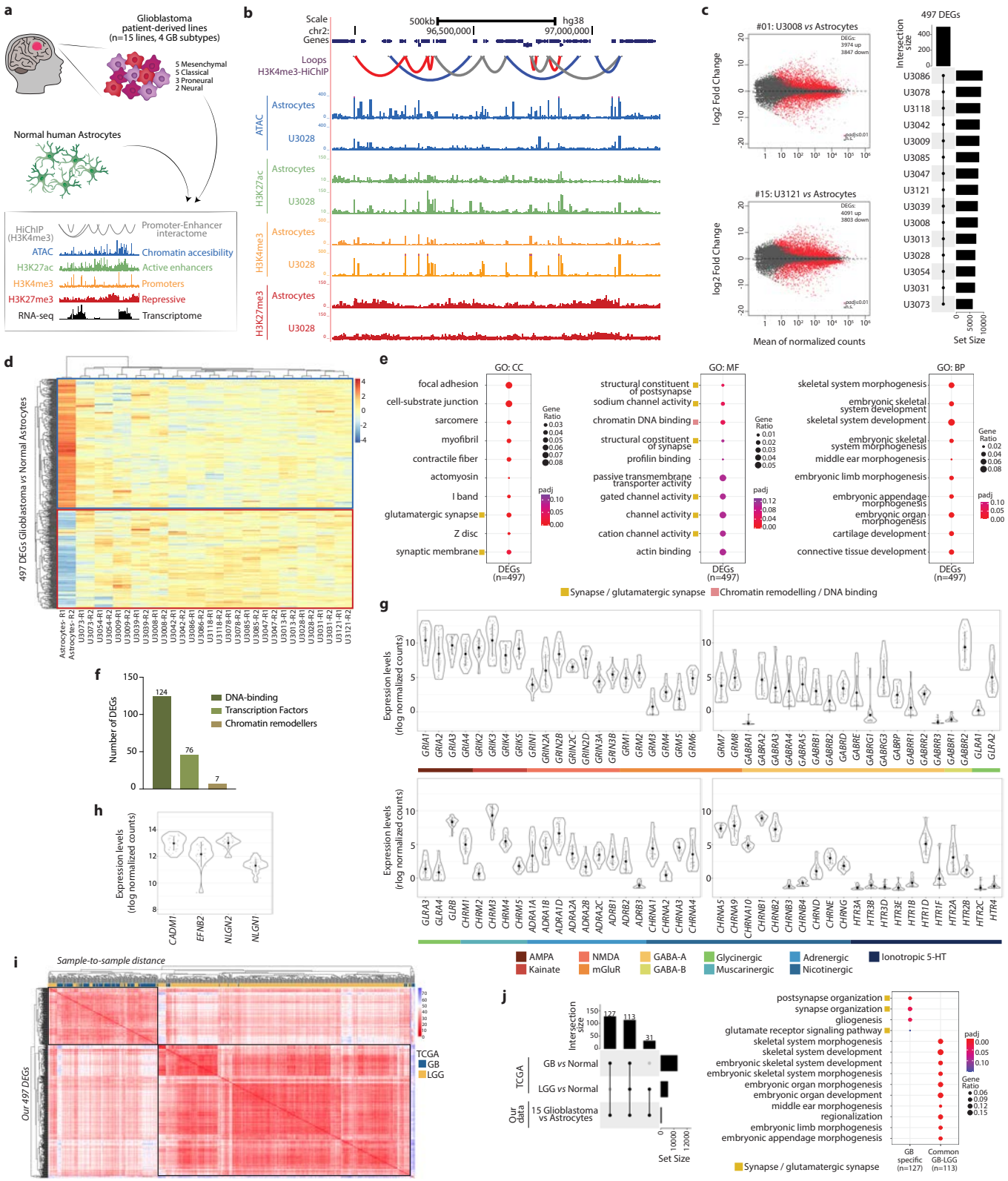

Figure 1: Gene expression changes common to all four glioblastoma subtypes relate to synapse organization, glutamatergic synapse and chromatin binding. a) Experimental workflow. b) Genomic distribution of HiChIP loops, chromatin accessible regions by ATAC, and H3K27ac, H3K4me3 and H3K27me3 peaks in normal astrocytes and one of the 15 glioblastoma cell lines (U3028). c) Differentially expressed genes (DEGs, red dots) in two representative glioblastoma lines *vs* normal astrocytes (left) and intersection of the 15 pairwise differential expression analysis resulting in 497 DEGs (right). d) Expression of 497 DEGs in all 15 glioblastoma lines and normal astrocytes as determined by RNA-seq (rlog normalized counts). e) Top 10 Gene Ontology terms enriched in the 497 DEGs. f) Number of DEGs annotated as DNA-binding, transcription factors or chromatin remodelers. g-h) Expression of neurotransmitter receptor genes (g) and synaptogenesis markers (h) in the 15 glioblastoma lines. i) Sample-to-sample distance for TCGA samples annotated as GB (glioblastoma, n=156) or LGG (lower grade glioma, n=511). j) Intersections between our 497 DEGs and the differential expressed genes from TCGA tumour samples, either GB *vs* normal or LGG *vs* normal tissue (left). Top 10 GO terms enriched in the 127 GB-specific genes or 113 genes common to GB and LGG (right).

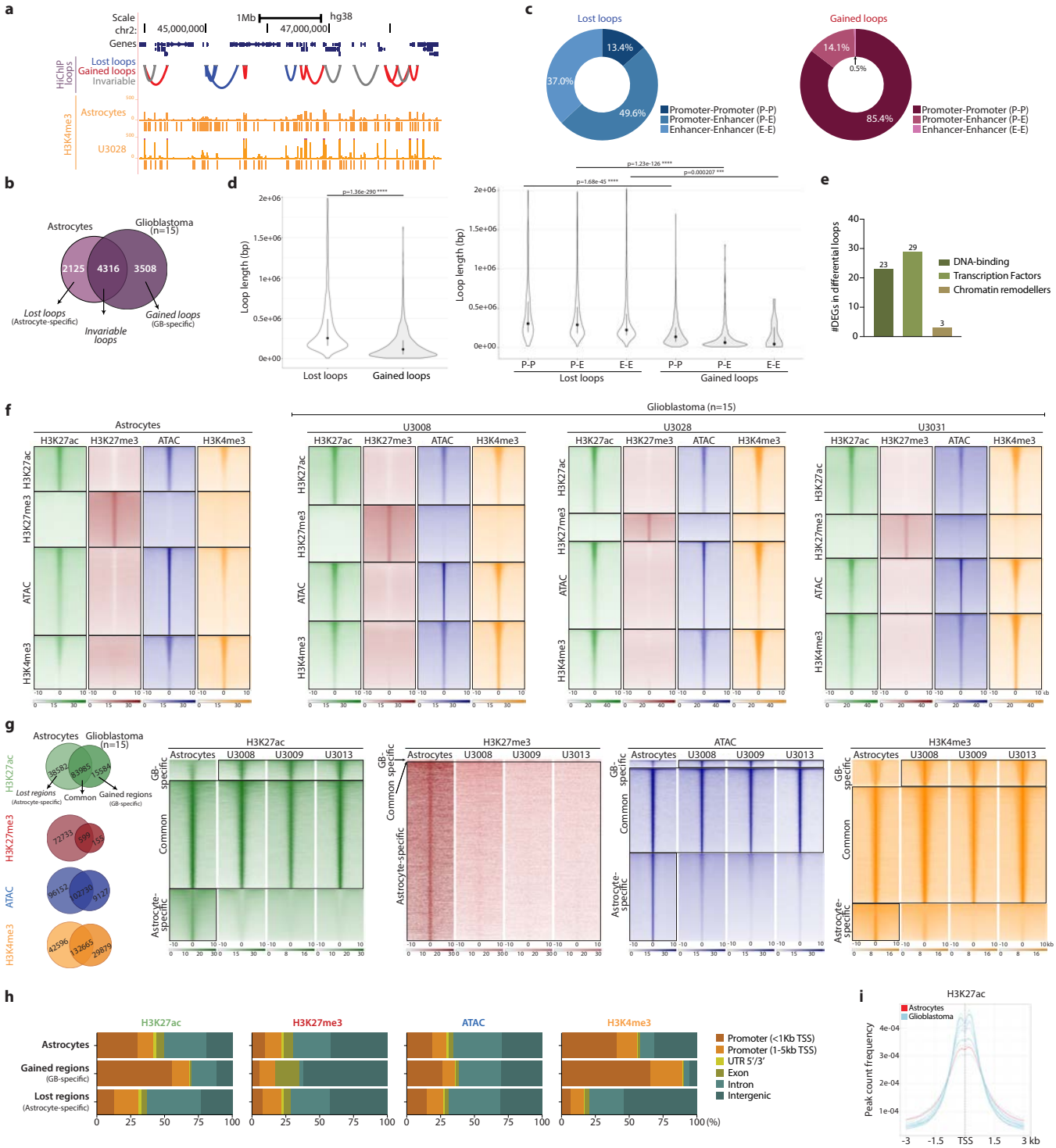

Figure 2: Loss of long-range regulatory interactions and changes in the regulatory landscape in glioblastoma. a) Distribution of HiChIP loops and H3K4me3 peaks in a region of chromosome 2. b) Intersection of HiChIP loops in the 15 glioblastoma lines and normal astrocytes defines lost loops ("astrocyte-specific") and gained loops ("GB-specific") in glioblastoma. c) Annotation of lost and gained loops as P-P, P-E or E-E loops. d) Length (bp) of lost and gained loops (t-test, Benjamini correction). e) Number of DEGs at the anchors of differential loops annotated as DNA-binding, transcription factors or chromatin remodelers. f) Read distribution of histone marks and ATAC around the indicated ±10kb regions in astrocytes and three representative glioblastoma lines. g) Redistribution of histone marks and ATAC regions in glioblastoma. h) Genomic annotation of differential histone peaks and ATAC regions in glioblastoma *vs* normal astrocytes. i) H3K27ac peak count frequency around the TSSs.

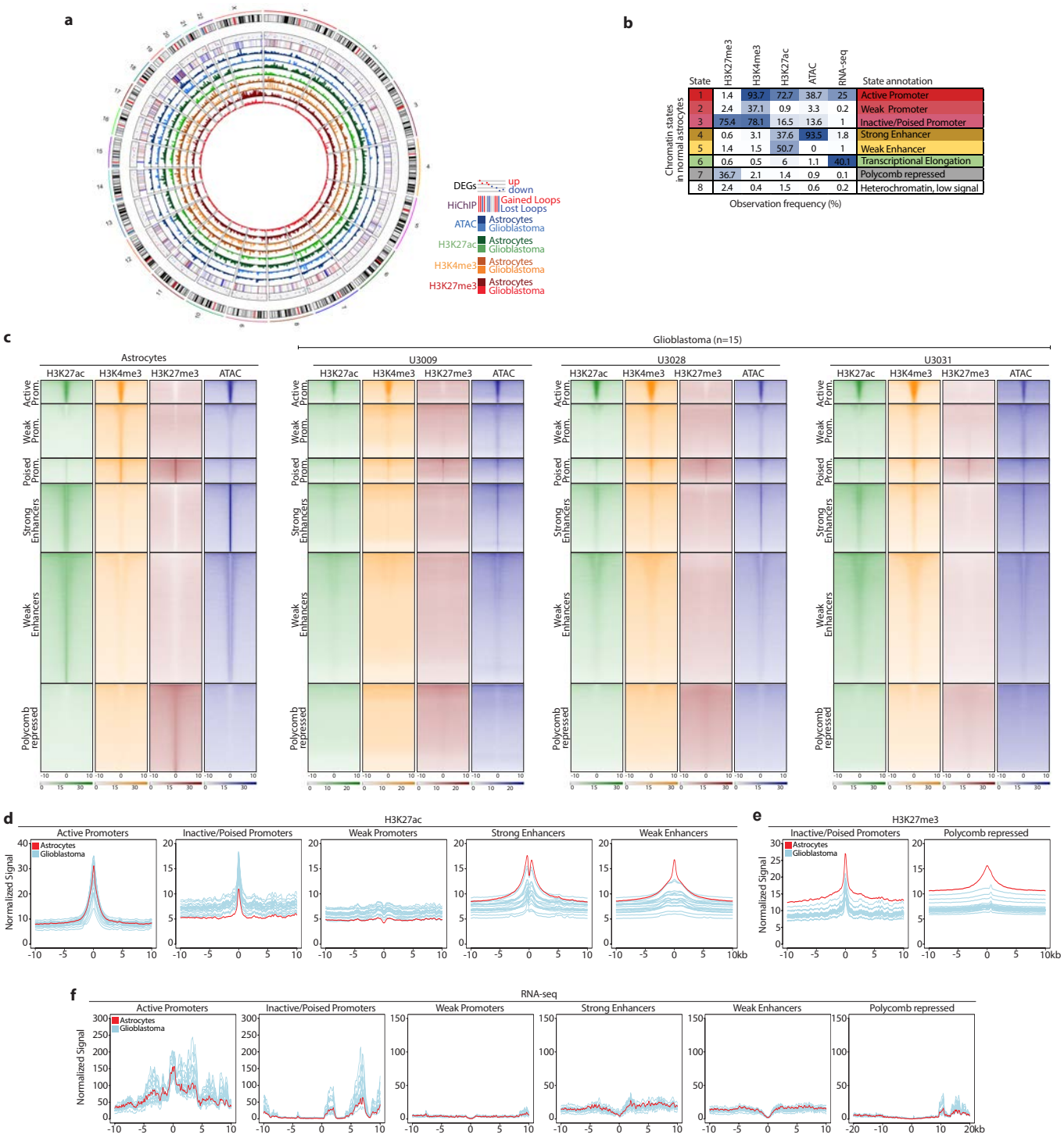

Figure 3: Remodeling of the regulatory landscape in glioblastoma includes reduction of active marks at enhancers and activation of promoters. a) Genome-wide integration of all the multi-omics data. b) Chromatin states defined by chromHMM in normal astrocytes. c) Read distribution of histone marks and ATAC across the various chromatin states in astrocytes and three representative glioblastoma lines. d-f) Density plots representing the normalized H3K27ac (d), H3K27me3 (e) and RNA-seq (f) signal around the astrocytes' chromatins states in glioblastoma (blue) *vs* astrocytes (red).

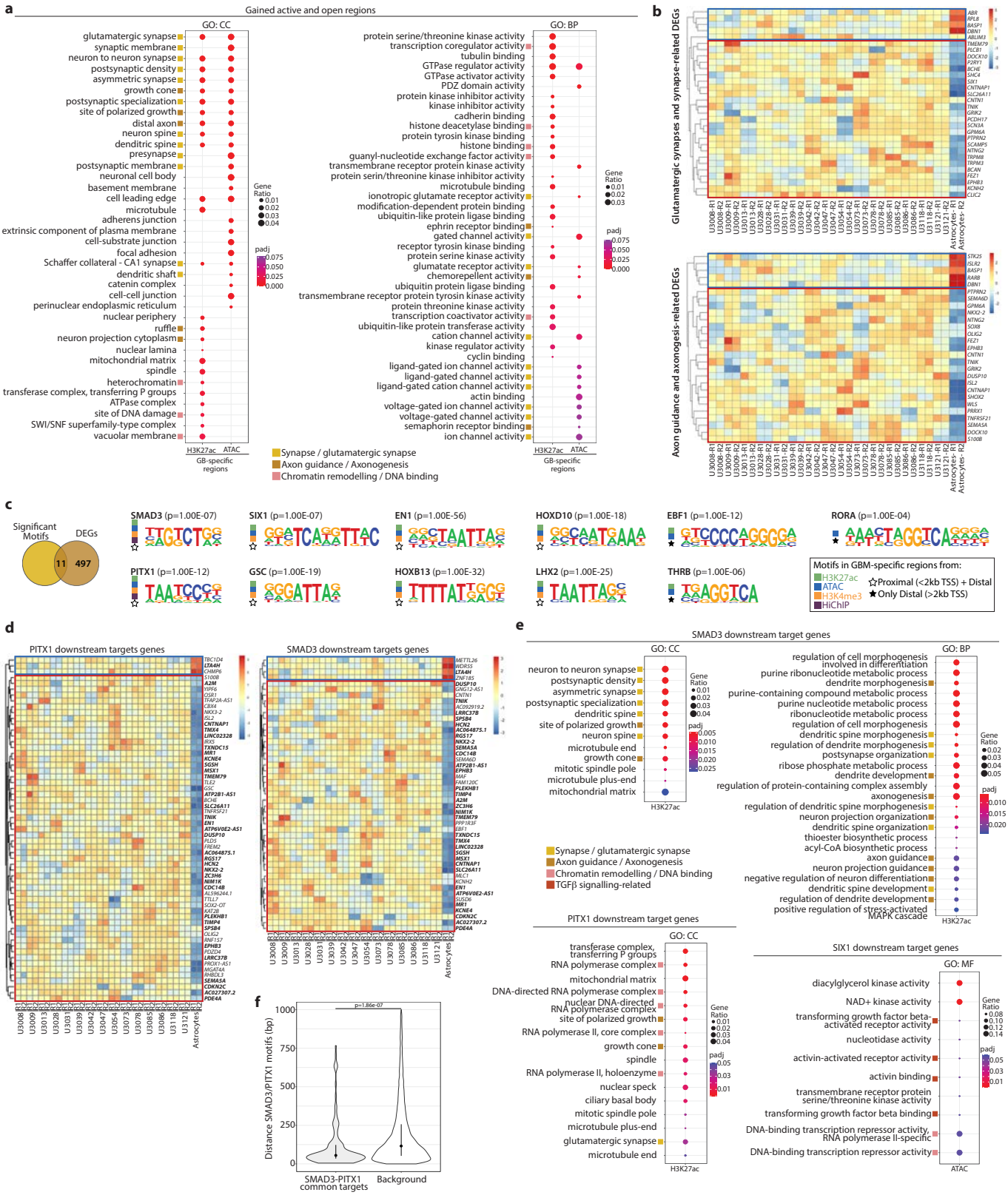

Figure 4: SMAD3 and PITX1 regulatory networks control genes associated to (glutamatergic) synapse organization and axonogenesis in glioblastoma. a) Top 25 GO terms enriched for genes proximal to gained active and open regions in glioblastoma (peaks <2kb TSS). b) Expression of DEGs related to synapse and glutamatergic synapse (top), and axon guidance and axonogenesis (bottom) located <2kb from a gained active/open peak. c) Intersection of the 497 DEGs with the HOMER significantly enriched motifs at the gained regions or anchors of differential loops identifies 11 key TFs. d) Expression of PITX1 and SMAD3 downstream target genes (i.e., motif enrichment at a differential peak <2kb TSS) among the DEGs in glioblastoma *vs* normal astrocytes (common targets in bold). e) Top GO terms enriched for SMAD3, PITX1 and SIX1 proximal downstream target genes. f) Distance between SMAD3 and PITX1 motifs at the promoters of the 33 common SMAD3/PITX1 target genes (left, median=56bp) *vs* background model (right, median=124bp).

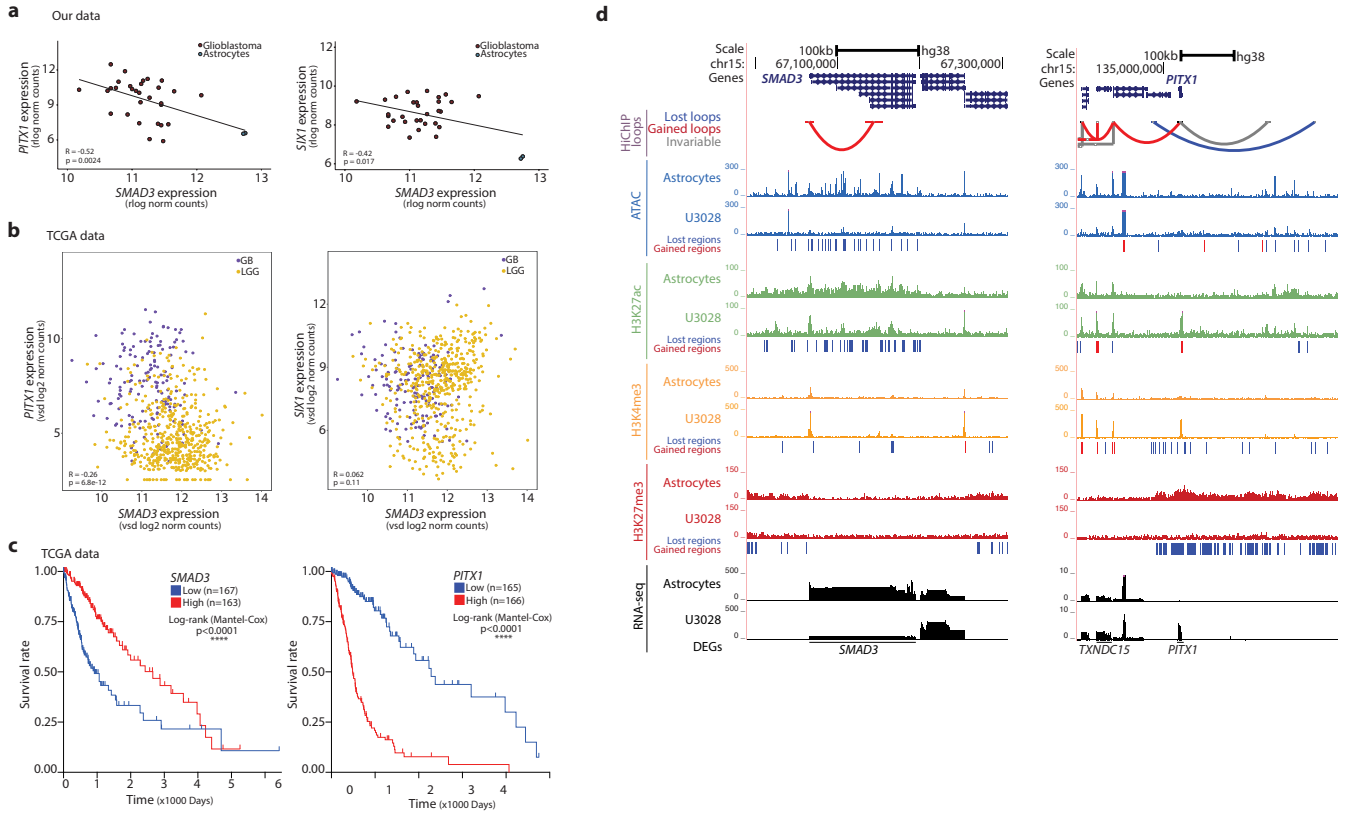

Figure 5: Regulatory alterations in the SMAD3 and PITX1 loci accompanied by inversely correlated gene expression and association to lower survival in patients. a-b) Scatterplots showing co-expression of SMAD3-PITX1 (left) or SMAD3-SIX1 (right) expressed as normalized counts in our data (a) and TCGA datasets (b)(Pearson correlations). c) Kaplan-Meier survival curves plotted for patients stratified by quartiles of SMAD3 or PITX1 expression (TCGA data) (log-rank Mantel-Cox test). d) Changes in the enhancer landscape and promoter-enhancer interactome at the SMAD3 and PITX1 loci (U3028 depicted as representative glioblastoma line).

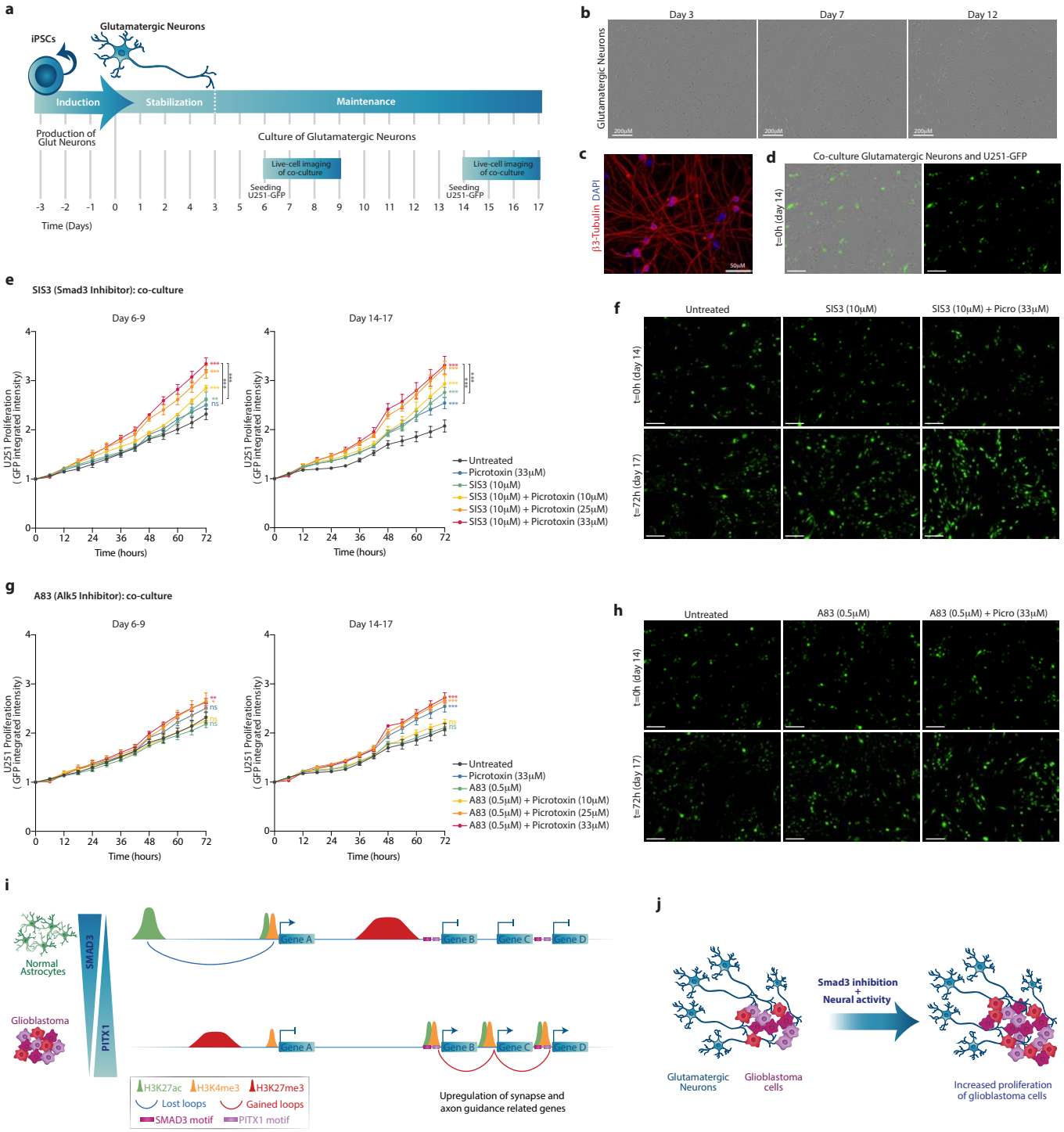

Figure 6: SMAD3 inhibition and neuronal activity cooperate to promote proliferation of glioblastoma cells in co-culture with glutamatergic neurons. a) Workflow to reprogram glutamatergic neurons from iPSCs, establish a co-culture with GFP-labelled U251 glioblastoma cells and live-cell image acquisition. b) Photomicrograph of glutamatergic neurons at days 3, 7 and 12. c) Glutamatergic neurons stained with an antibody against β3-Tubulin (red) (DAPI, blue). d) Photomicrographs of glutamatergic neurons and U251-GFP glioblastoma cells (green) in co-culture. e,g) Proliferation curves depicting the growth of U251 cells (measured as normalized GFP integrated intensity) in co-culture with glutamatergic neurons in the 72h after seeding at day 6 (left) or day 14 (right), while treated with either the SMAD3-specific inhibitor SIS3 (e) or the ALK5 inhibitor A83 (g), in combination with increasing concentrations of picrotoxin. (Multiple unpaired t-test, t=72h, (* $p<0.01$, ** $p<0.005$, *** $p<0.000005$, n=6-8). f,h) Representative images from the live-cell imaging proliferation assay of U251-GFP in co-culture with glutamatergic neurons, in the presence of either SIS3 (f) or A83 (h). i) Scheme illustrating the regulatory and topological changes in the glioblastoma genome including loss of long-range interactions, gain of promoter-promoter loops, redistribution of active chromatin marks towards SMAD3 and PITX1 binding motifs and upregulation of genes related to synapse organization, axon guidance and axonogenesis. j) Illustration depicting that Smad3 inhibition and stimulation of neural activity cooperate to promote proliferation of glioblastoma cells in co-culture with glutamatergic neurons.

a

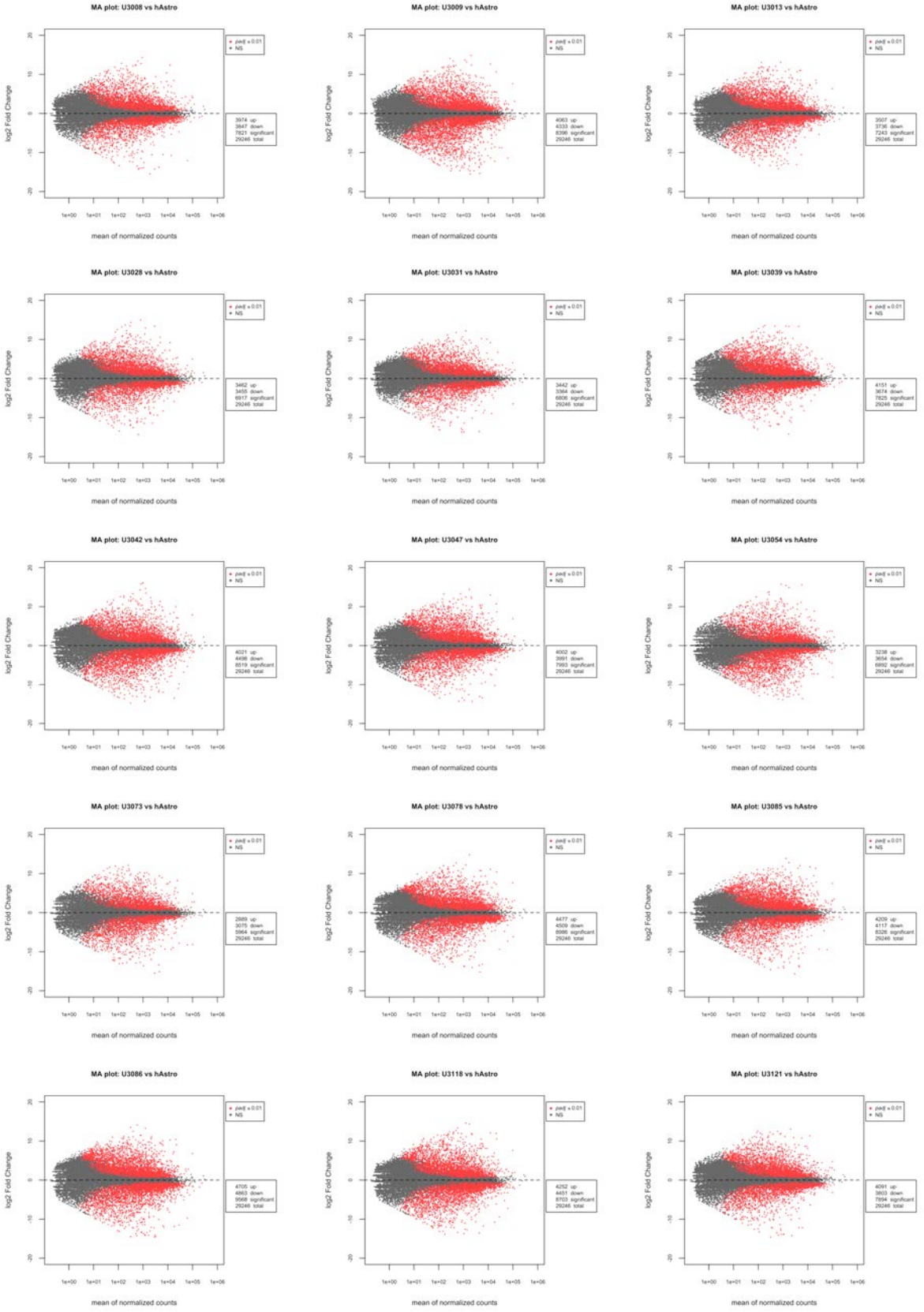

b

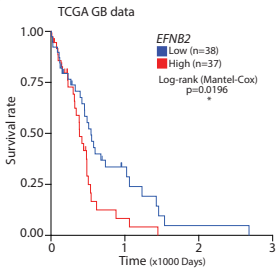

Supplementary Figure 1: a) MA plots showing genes differentially expressed (DEGs, red dots) in each of the 15 glioblastoma lines *vs* normal astrocytes. b) Kaplan-Meier survival curves plotted for patients stratified by quartiles of *EFNB2* expression (TCGA data) (log-rank Mantel-Cox test).

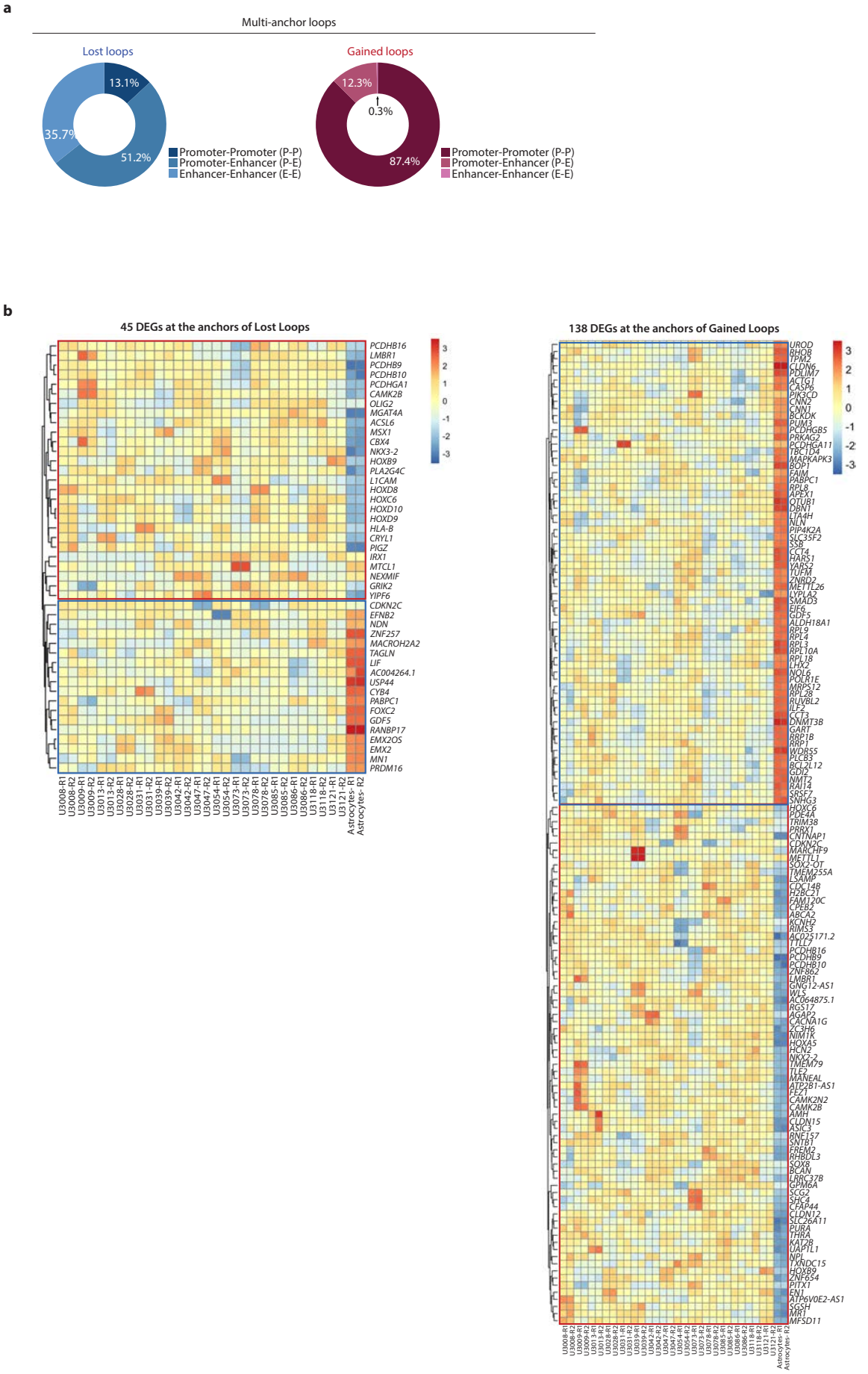

Supplementary Figure 2: a) Annotation of lost and gained multi-anchor loops as promoter-promoter, promoter-enhancer or enhancer-enhancer loops. b) Expression of 45 DEGs located at the anchors of lost loops (left) and 138 DEGs at the anchors of gained loops (right), in all 15 glioblastoma lines and normal astrocytes as determined by RNA-seq (rlog normalized counts).

a

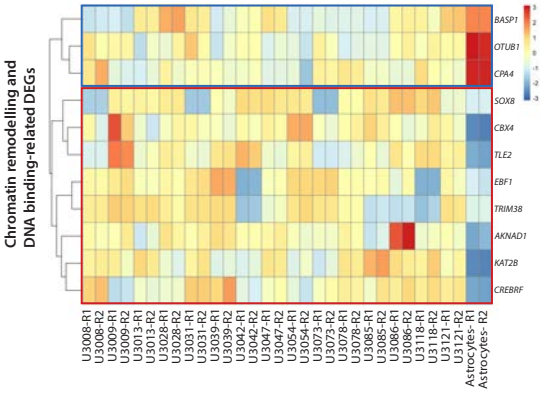

b

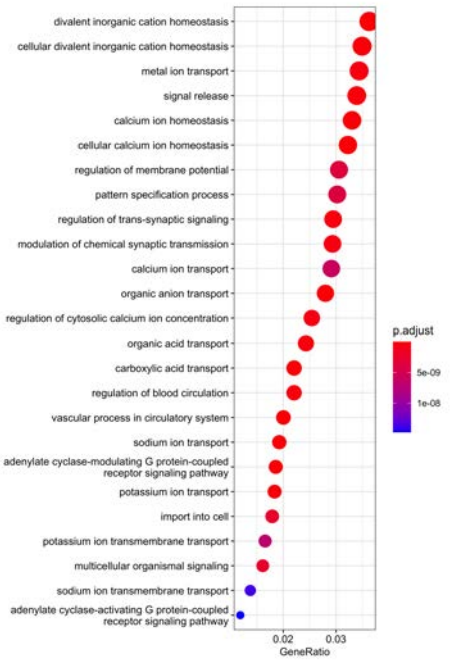

c

Proximal (<2kb TSS) gained regions (GB-specific):

			H3K27ac		ATAC		H3K4me3	
TF	Motif	Sequence	Motif Logo	p-value	Motif Logo	p-value	Motif Logo	p-value
En1	En1(Homeobox)/SUM149-EN1-ChIP-Seq(GSE120957)/Homer	NDCTAATTAS		1.00E-56		1.00E-34		1.00E-43
GSC	GSC(Homeobox)/FrogEmbryos-GSC-ChIP-Seq(DRA000576)/Homer	RGGATTAR		1.00E-19		1.00E-16		1.00E-52
HOXB13	HOXB13(Homeobox)/ProstateTumor-HOXB13-ChIP-Seq(GSE56288)/Homer	TTTTATKRGG		1.00E-32		1.00E-16		1.00E-31
HOXD10	Hoxd10(Homeobox)/ChickenMSG-Hoxd10.Flag-ChIP-Seq(GSE86088)/Homer	GGCMATGAAA		1.00E-18		1.00E-14		1.00E-14
LHX2	Lhx2(Homeobox)/HFSC-Lhx2-ChIP-Seq(GSE48068)/Homer	TAATTAGN		1.00E-25		1.00E-39		1.00E-31
PITX1	Pitx1(Homeobox)/Chicken-Pitx1-ChIP-Seq(GSE38910)/Homer	TAATCCCN		1.00E-12		1.00E-08		1.00E-10
SIX1	Six1(Homeobox)/Myoblast-Six1-ChIP-Chip(GSE20150)/Homer	GKVTCADRTTWC		1.00E-07		1.00E-02	-	-
SMAD3	Smad3(MAD)/NPC-Smad3-ChIP-Seq(GSE36673)/Homer	TWGTCTGV		1.00E-07		1.00E-09	-	-

d

Distal (>2kb TSS) gained regions (GB-specific):

			H3K27ac		ATAC		H3K4me3	
TF	Motif	Sequence	Motif Logo	p-value	Motif Logo	p-value	Motif Logo	p-value
En1	En1(Homeobox)/SUM149-EN1-ChIP-Seq(GSE120957)/Homer	NDCTAATTAS		1.00E-12		1.00E-14		1.00E-11
GSC	GSC(Homeobox)/FrogEmbryos-GSC-ChIP-Seq(DRA000576)/Homer	RGGATTAR		1.00E-20		1.00E-08		1.00E-09
HOXB13	HOXB13(Homeobox)/ProstateTumor-HOXB13-ChIP-Seq(GSE56288)/Homer	TTTTATKRGG		1.00E-12		1.00E-20		1.00E-25
HOXD10	Hoxd10(Homeobox)/ChickenMSG-Hoxd10.Flag-ChIP-Seq(GSE86088)/Homer	GGCMATGAAA		1.00E-08		1.00E-32		1.00E-16
LHX2	Lhx2(Homeobox)/HFSC-Lhx2-ChIP-Seq(GSE48068)/Homer	TAATTAGN		1.00E-19		1.00E-34		1.00E-17
PITX1	Pitx1:Ebox(Homeobox,bHLH)/Hindlimb-Pitx1-ChIP-Seq(GSE41591)/Homer	YTAATTRAWWCCAGATGT		1.00E-23	-	-		1.00E-04
SIX1	Six1(Homeobox)/Myoblast-Six1-ChIP-Chip(GSE20150)/Homer	GKVTCADRTTWC		1.00E-03		1.00E-15		1.00E-05
SMAD3	Smad3(MAD)/NPC-Smad3-ChIP-Seq(GSE36673)/Homer	TWGTCTGV		1.00E-23		1.00E-17		1.00E-05
RORa	RORa(NR)/Liver-Rora-ChIP-Seq(GSE101115)/Homer	AAWCTAGGTCARDNN	-	-		1.00E-04	-	-
EBF1	EBF1(EBF)/Near-E2A-ChIP-Seq(GSE21512)/Homer	GTCCCCWGGGGA		1.00E-12		1.00E-04	-	-
THRB	THRb(NR)/Liver-NR1A2-ChIP-Seq(GSE52613)/Homer	TRAGGTCA		1.00E-06		1.00E-02	-	-

e

HiChIP (anchors of differential loops)

TF	Motif	Sequence	Motif Logo	p-value
PITX1	Pitx1(Homeobox)/Chicken-Pitx1-ChIP-Seq(GSE38910)/Homer	TAATCCCN		1.00E-12
SMAD3	Smad3(MAD)/NPC-Smad3-ChIP-Seq(GSE36673)/Homer	TWGTCTGV		1.00E-20

Supplementary Figure 3: a) Expression of DEGs related to chromatin remodelling and DNA binding located <2kb from a gained active/open peak. b) Top 25 GO terms enriched for the genes proximal to the lost repressive regions in glioblastoma (peaks <2kb TSS). c,d) Summary of the TF binding motifs enriched at proximal (<2kb TSS) (c) or distal (>2kb TSS) (d) gained regions in glioblastoma for H3K27ac, ATAC and H3K4me3, including motif, sequence and p-values. e) Summary of the TF binding motifs enriched at the anchors of the differential loops, including motif, sequence and p-value.

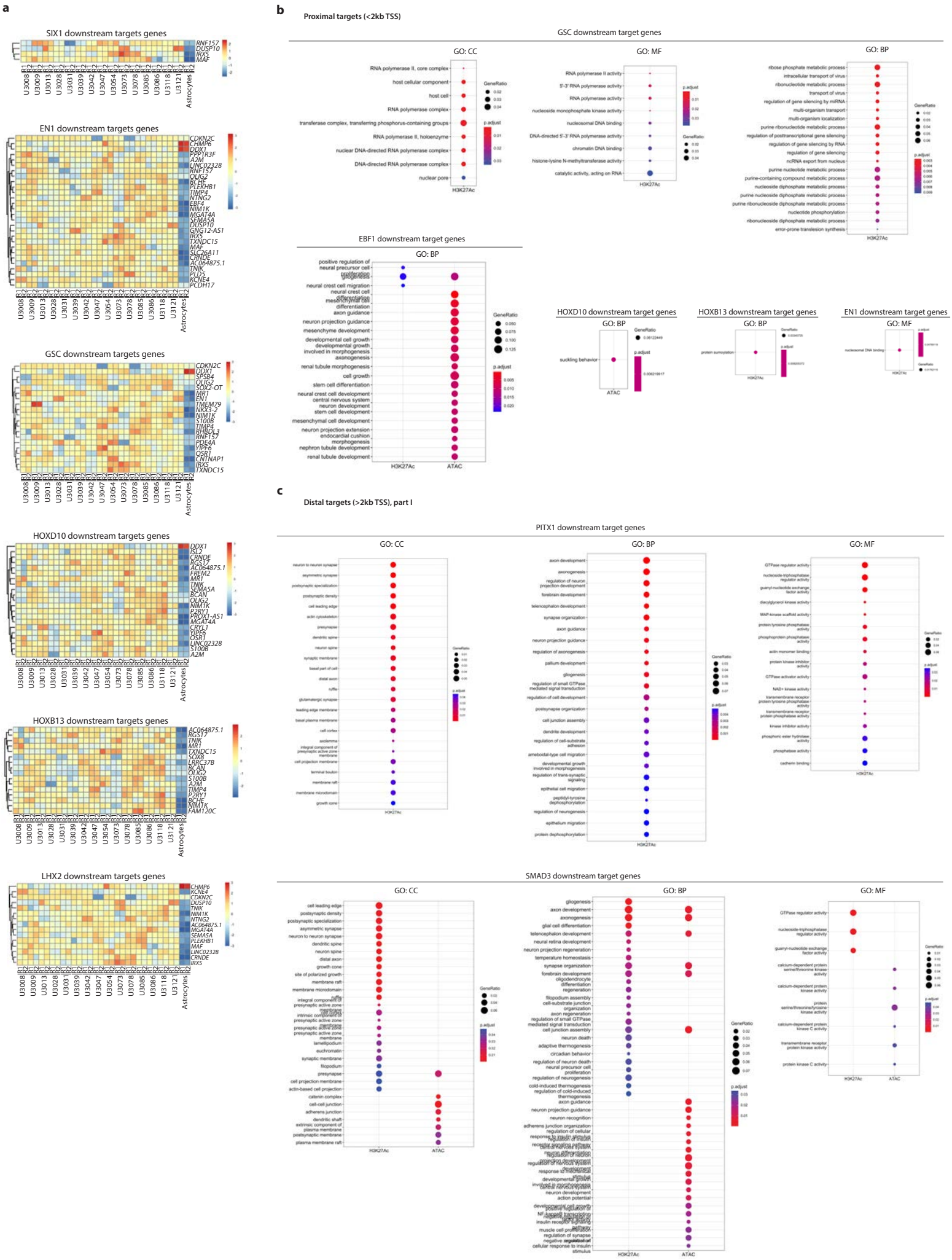

Supplementary Figure 4: a) Expression of the SIX1, EN1, GSC, HOXD10, HOXB13 and LHX2 downstream target genes (i.e., motif enrichment at a differential peak <2kb TSS) that are DEGs in glioblastoma *vs* normal astrocytes. b) GO terms enriched for the GSC, EBF1, HOXD10, EN1 and HOXB13 proximal downstream target genes (<2kb TSS). c) GO terms enriched for the PITX1 and SMAD3 distal downstream target genes (>2kb TSS).

a

Distal targets (>2kb TSS), part II

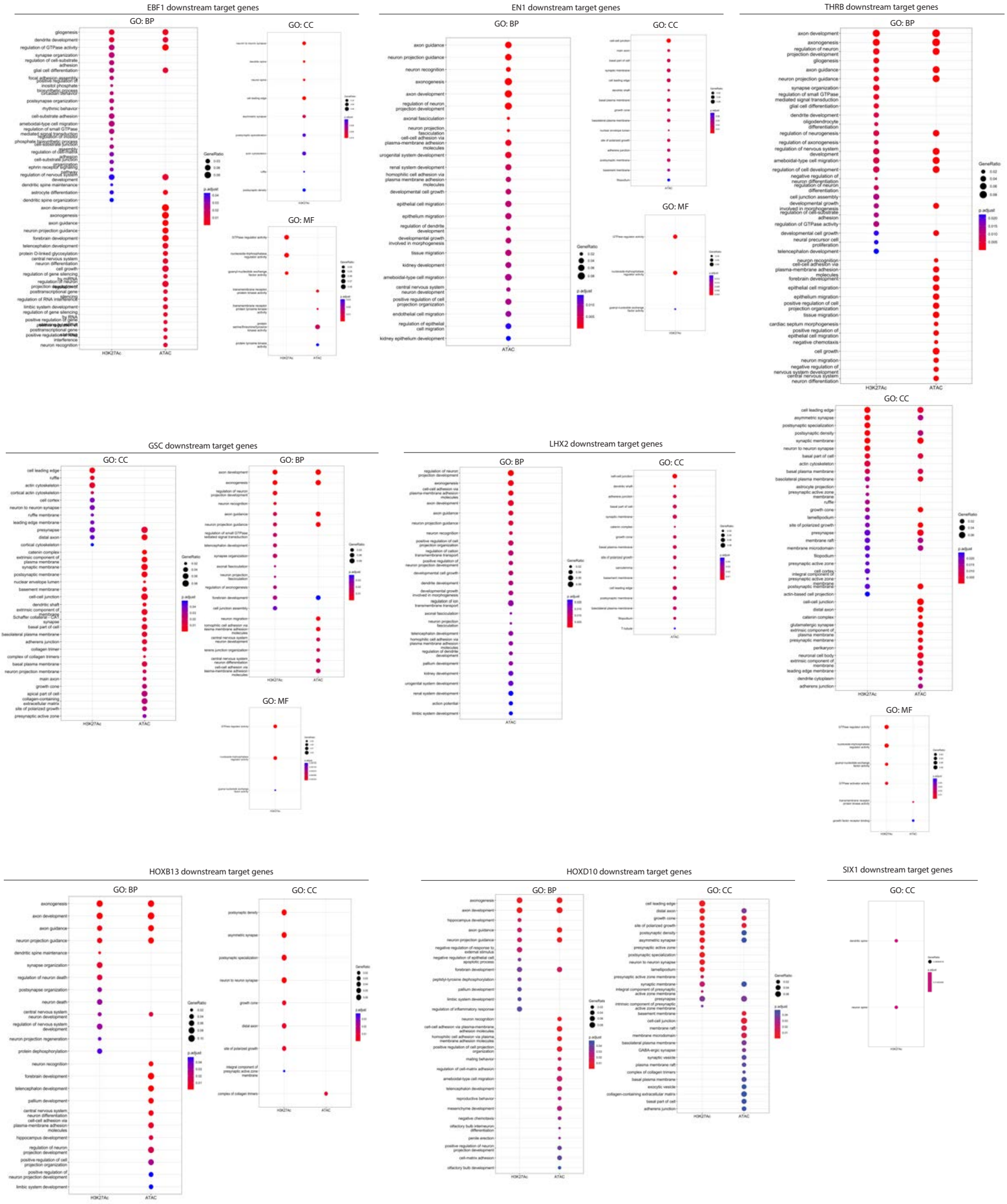

Supplementary Figure 5: a) GO terms enriched for the EBF1, EN1, THRB, GSC, LHX2, HOXB13, HOXD10 and SIX1 distal downstream target genes (>2kb TSS).

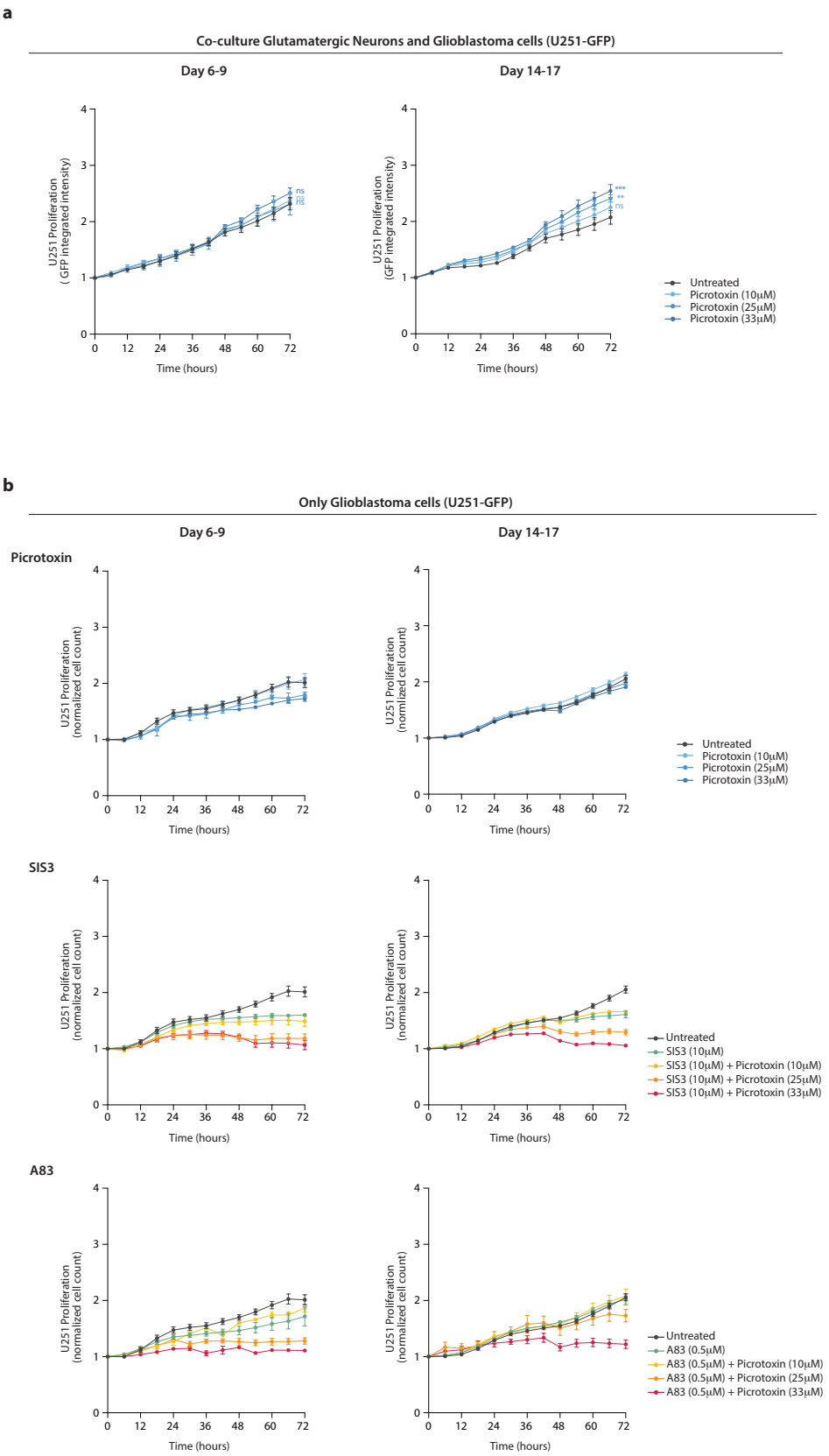

Supplementary Figure 6: a) Proliferation curves depicting the growth of U251 cells (measured as normalized GFP integrated intensity) in co-culture with glutamatergic neurons in the 72h after seeding at day 6 (left) or day 14 (right) at different concentrations of picrotoxin. (Multiple unpaired t-test, t=72h, (* $p<0.01$, ** $p<0.005$, *** $p<0.000005$). (n=6-8). b) Proliferation curves of U251 cells in the absence of neurons (measured as normalized cell count) in the 72h after seeding at day 6 (left) or day 14 (right) and under the same drug treatments as used in Figure 6 e,g.